THE PENNSYLVANIA STATE UNIVERSITY
SCHREYER HONORS COLLEGE

DEPARTMENT OF ASTRONOMY & ASTROPHYSICS

# UTILIZING SWIFT-XRT DATA TO IDENTIFY SOURCE CLASSES IN FERMI UNASSOCIATED OBJECTS

MATTHEW PRYAL
SPRING 2015

A thesis
submitted in partial fulfillment
of the requirements
for a baccalaureate degree
in Astronomy & Astrophysics
with honors in Astronomy & Astrophysics

Reviewed and approved* by the following:

Abraham Falcone
Senior Scientist and Professor of Astronomy & Astrophysics
Thesis Supervisor

Alex Wolszczan
Evan Pugh Professor of Astronomy & Astrophysics
Honors Adviser

* Signatures are on file in the Schreyer Honors College.

# ABSTRACT

The Large Area Telescope on board the *Fermi Gamma-Ray Space Telescope* has revolutionized the detection and identification of gamma-ray emitting astrophysical objects since the launch of *Fermi* in 2008. Gamma-rays are the highest energy photons observed in the universe and our understanding of objects that emit gamma-rays is essential to our understanding of physics at its greatest limits. The 1FGL, 2FGL, and 3FGL *Fermi* catalogs outline the identification of over 2000 gamma-ray emitting objects such as blazars and pulsars, but there still remains many unassociated objects in the *Fermi* catalogs. In this thesis we attempt to statistically show associations of these *Fermi* unassociated objects in the 1FGL and 2FGL catalogs by utilizing data mining and machine learning techniques to find distinct separations in the properties of known blazars and pulsars. Our analysis is unique in that we will be utilizing known X-ray fluxes for the unassociated objects observed by the *Swift* X-ray Telescope in addition to the gamma-ray properties available in the *Fermi* catalogs. Our analysis shows distinct separations in the gamma-ray properties of known blazars and pulsars when compared to X-ray flux and we were able to suggest possible associations to 136 previously unassociated *Fermi* objects.

# TABLE OF CONTENTS

# LIST OF FIGURES

# LIST OF TABLES

## ACKNOWLEDGEMENTS

I would like to sincerely thank Dr. Abe Falcone for all the guidance and opportunities he has provided me over the past three years as my research adviser and thesis supervisor in addition to the weekly discussions and insights about my research and academic life. I would like to thank Dr. Eric Feigelson for helping me to understand the astrostatistics and R techniques utilized in completing this thesis. I would like to thank my honors advisor Dr. Alex Wolszczan for reading through my thesis and offering necessary advice towards its completion. I would like to thank the Penn State Department of Astronomy & Astrophysics and the Schreyer's Honors College for providing me with the necessary skills to complete my thesis and succeed in my planned future. And finally, I would like to thank my family and friends, whom without my thesis would have been completed much earlier.

# Chapter 1

## Introduction

With the launch of OSO 3 in 1967 the detection and identification of gamma-ray emitting objects (Kraushaar et al., 1972) has been at the forefront of high-energy astrophysical research. Gamma-rays constitute the highest energy band of the electromagnetic spectrum and typically have energy greater than approximately 100 keV. Gamma-ray emitting objects are particularly interesting because they push the limits of physics and therefore our understanding of how these objects emit such high-energy light is essential to our understanding of physics as a whole. Identification of these high-energy gamma-ray detections with real astrophysical sources has typically been difficult due the relatively small amount gamma-ray photons that reach orbiting or ground based detectors, which results in large positional errors in their measured locations. Early gamma-ray detectors, such as COS-B (Bignami et al., 1975) and EGRET, on board the *Compton Gamma-Ray Observatory* (Thompson et al., 1993), also had a large amount of spurious detections as was determined by follow-up observations.

The *Fermi* Gamma-ray Space Telescope (Atwood et al., 2009), launched on 2008 June 11 initially as the *Gamma-ray Large Area Space Telescope* (GLAST), revolutionized the detection and identification of these high-energy gamma-ray sources. The primary instrument on board *Fermi*, its Large Area Telescope (LAT; Atwood et al., 2009) is often considered a successor to EGRET. The *Fermi*-LAT is sensitive to photons with energies that range from 100 MeV to about

300 GeV, which is much more sensitive than EGRET or any of the other gamma-ray detectors were able to observe.

The *Fermi*-LAT has been surveying the entire sky since its launch in 2008 and due to its deep and uniform exposures, good angular resolution relative to other gamma-ray detectors, and stable response, it is the perfect tool for analyzing a large number of gamma-ray emitting sources. To date there have been three *Fermi* catalogs listing the gamma-ray sources detected and offering possible associations for the observed objects when possible. The *Fermi*-LAT First Source Catalog (1FGL; Abdo et al., 2010b) reports a detection of 1451 gamma-ray emitting objects during the first 11 months of the science phase of the mission. The *Fermi*-LAT Second Source Catalog (2FGL; Nolan et al., 2012) reports a detection of 1873 gamma-ray emitting objects during the first 24 months of the science phase of the mission. The most recently released *Fermi* catalog, the Third Source Catalog (3FGL; Acero et al., 2015) reports a detection of 3033 gamma-ray emitting objects during the first four years of the science phase of the mission.

Of the 1451 gamma-ray detections reported in the 1FGL catalog, 821 objects were shown to be associated with a possible counterparts based on correlated variability at other wavelengths, or on spin or orbital periodicity, while 630 objects remained unassociated. Of the 821 1FGL objects associated with a counterpart, 698 were extragalactic in origin and 123 were Galactic. For the 2FGL catalog 575 objects were unassociated and for the 3FGL catalog 992 objects were unassociated with similar percentages compared to the 1FGL catalog to objects being galactic versus extragalactic. The extragalactic objects observed in all the catalogs were typically associated with an Active Galactic Nucleus (AGN), in particular a blazar, whereas the Galactic objects were typically associated with pulsars. The physical processes for blazars and pulsars that result in the emission of gamma-rays are discussed in more detail below.

The purpose of this thesis is to investigate the parameter space of *Fermi* variables with an emphasis on observed X-ray flux to determine what variables are dominant in discriminating the known blazars and pulsars. This type of statistical analysis, sometimes referred to as data mining and machine learning, has been attempted in the past with the 1FGL and 2FGL data (Ackermann et al. 2012; Mirabal et al. 2012; Hassan et al. 2013; Doert & Errando 2014) and has shown success. In our data mining and machine learning analysis we further constrain the unassociated *Fermi* objects by utilizing X-ray data from the *Swift* X-ray Telescope (XRT; Burrows et al., 2005). This additional constraint of X-ray data has never been included in past attempts at associating the *Fermi* unassociated sources. By applying X-ray data to the observed gamma-ray *Fermi* properties, our data mining and machine learning techniques will be much stronger and provide greater confidence in calculated results.

Blazars are a class of AGNs that have their relativistic jet pointed in a direction that is close Earth's line of sight. The spectral energy distribution (SED) of blazars consists of two distinct components that result in large bumps in the SED with the first typically due to X-ray photons and the second due to the gamma-ray photons (Abdo et al., 2010a). This first bump in the SED due to X-ray flux is typically modeled as being from synchrotron emission as electrons are accelerated along the relativistic jet of the blazar. The gamma-ray bump is typically modeled as being from inverse Compton emission, with seed photons sometimes from synchrotron emission. An example of the blazar SED can be seen in Figure 1 below.

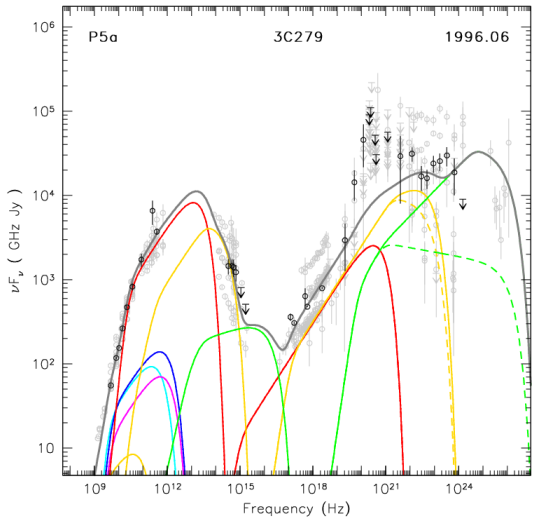


**Figure 1: Spectral energy distribution of 3C279 (Türler & Björnsson 2011)**

Pulsars are rapidly rotating neutron stars that can sometimes rotate faster than once every millisecond. As with the blazars, pulsars also show a distinct double hump in their SED with the X-rays typically modeled due to synchrotron radiation and gamma-rays are modeled by what is called "synchro –curvature radiation" (Zhang & Cheng 2003).

The emissions of X-ray and gamma-ray emission in blazars and pulsars has been shown to be correlated on multiple occasions (Catanese et al., 1997; Pian et al., 1998; Sambruna et al., 2000; Donnarumma et al., 2009). This correlation between X-rays and gamma-rays in astrophysical processes has motivated our introduction of X-ray data to the *Fermi* data because it would have a strong impact on finding separations in the sources.

For our analysis, we compare plots of the different observed variables provided in the *Fermi* catalog as well as our X-ray data in the search for distinctions between the known blazars and pulsars, which we refer to as our training sets. On each of our plots we over plot the unassociated objects, or the test set, in the search for possible associations. These plots can then be systematically compared through machine learning techniques such as principal component

analysis (PCA), classification trees (CT) techniques, and in our case k-nearest neighbor tests (KNN) to associate the unassociated objects whenever possible.

This thesis will help aid in the decision of future observations of unassociated *Fermi* objects in the search for counterparts by allowing observers to know what objects they are likely to find counterparts for. The *Fermi*-LAT is discussed in more detail in Chapter 2, the *Swift*-XRT is outlined in Chapter 3, our data set that includes the training sets and test set is outlined in Chapter 4, our methodology for association that includes the data mining techniques utilized is discussed in Chapter 5, the results from our data mining analysis which includes relevant plots is included in Chapter 6, and our conclusion that includes a discussion on the implication of the results is included in Chapter 7. We also provide relevant figures in Appendix A and Appendix B at the end of this thesis.

# Chapter 2

## The *Fermi* Large Area Telescope

The *Fermi Gamma-Ray Space Telescope* (*Fermi*; Atwood et al., 2009, Figure 2) was a major technological advancement in the study of the highest energy band of the electromagnetic spectrum: gamma-rays. The main operator of *Fermi* is NASA and the U.S. Department of Energy with major contributions from the French National Center for Space Studies (CNES), the German Aerospace Center (DLR), the Italian Space Agency (ISA), the Japan Aerospace Exploration Agency (JAXA), and the Swedish National Space Board (SNSB), thus making it an international and multi-agency collaboration. The *Fermi* science mission is controlled out of NASA Goddard and began its planned ten-year science mission in 2008.

**Figure 2: This image shows an artist interpretation of Fermi in Earth orbit via NASA's Goddard Space Flight Center.**

*Fermi* consists of two science instruments: its primary instrument, the Large Area Telescope (LAT; Atwood et al., 2009), and the Gamma-ray Burst Monitor (GBM; Meegan et al., 2009). Together these instruments have mapped the gamma-ray sky and significantly increased

our understanding of the physical processes behind the observed gamma-ray emitting objects such as AGNs, pulsars, pulsar wind nebulae (PWN), and gamma-ray bursts.

The primary focus of the GBM is the detection and analysis of gamma-ray bursts throughout the universe. The GBM is unique in that it can observe these gamma-ray bursts from part of the energy range observed by the LAT as well as collecting information all the way down to the hard X-ray range. The GBM performs this analysis through the use of a primary objective to extend the range that bursts are observed and a secondary objective to orient the spacecraft to the burst location.

The LAT (Figure 3) is a gamma-ray telescope with a wide field of view that can detect photons in the 20 MeV to 300 GeV range. This wide field of view, that is approximately 2.4 steradians in size or about 20% of the sky, allows the LAT to observe the entire sky every three hours. This constant observation of the gamma-ray sky allows astronomers to measure how many gamma-ray emitting objects evolve over time and thus get a greater understanding of the physical processes at work.

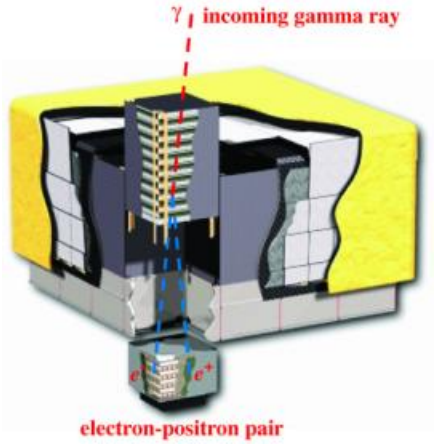


**Figure 3: Fermi-LAT cutaway showing how the gamma-rays are detected. [Atwood et al., 2009]**

The LAT is specifically a pair-conversion telescope, which means that it allows gamma-rays to impact its surface to create electron-positron pairs and then uses a detector to observe the

pair production rather than the gamma-ray itself. This aspect of the telescope and other gamma-ray detectors differs from the common perception of a telescope because gamma-rays cannot be simply reflected or refracted and thus must be measured in this manner. The LAT also has a precision tracker and calorimeter consisting of a 4 × 4 array of 16 modules, a segmented anticoincidence detector that covers the tracker array, and a programmable trigger and data acquisition system. The arrangement of the calorimeter modules as discussed in Atwood et al., 2009 provide longitudinal and transverse information about the energy pattern in the electron-positron pairs, which gives precise location detections of the gamma-ray emitting objects. The aspect ratio of the LAT tracker is 0.4, which allows for the large field of view and allows the highest detection of pair conversion events.

*Fermi* has been extremely successful since its launch and has significantly expanded our knowledge of the gamma-ray sky. As the *Fermi* team continues to observe deeper and deeper into the gamma-ray sky (Figure 4) and creates catalogs in addition to the 1FGL, 2FGL, and 3FGL catalogs our understanding of the physical processes behind these objects will become much more clear. Utilizing the *Fermi* data in multi-wavelength analyses such as the one we are doing in this thesis will become essential to gaining a complete understanding of the universe.

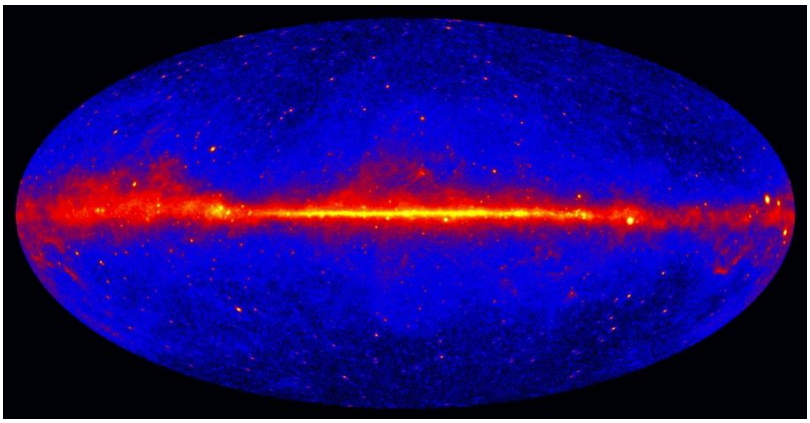

**Figure 4: This image shows the distribution of gamma-ray emitting objects throughout space is known as the 3FGL all sky map, with the line through the center signifying the galactic plane. [Acero et al., 2015]**

# Chapter 3

## The *Swift* X-ray Telescope

The *Swift* X-ray telescope (XRT; Burrows et al., 2005; Figure 5, right) is one of the three primary instruments on board the *Swift* Gamma-Ray Explorer (Gehrels et al., 2004; Figure 5). *Swift* was launched into orbit on 20 November 2004 and along with the XRT consists of the Burst Alert Telescope (BAT; Barthelmy et al., 2004) and the Ultraviolet/Optical Telescope (UVOT; Roming et al., 2005). NASA and its Goddard Space Flight Center in addition to agencies in the United States, Italy, and the United Kingdom developed the mission. The primary mission of *Swift* is the detection and quick multi-wavelength observation of gamma ray bursts to help explain the physical processes behind these high-energy processes. The mission control center is operated at the Pennsylvania State University, who was a major contributor to the launch of the spacecraft.

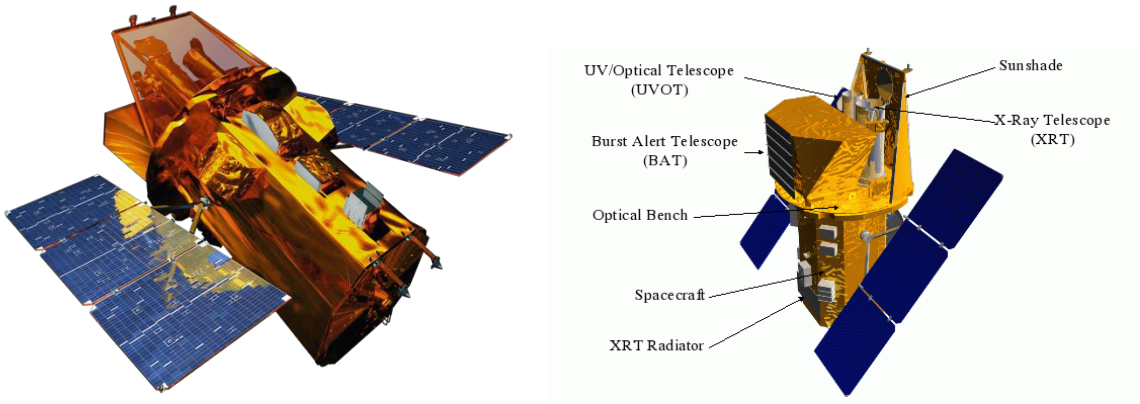


**Figure 5: The Swift Gamma Ray Burst Explorer (left) with instruments labeled (right) [images via NASA]**

In particular, the XRT is an X-ray imaging spectrometer sensitive to photons in the 0.2-10.0 keV energy range. The XRT is able to observe photons in this band through the use of a grazing incidence Wolter I telescope to focus X-rays onto a thermoelectrically cooled CCD as

discussed in Burrows et al., 2005. The set-up and diagram of the XRT and the path it takes to observe the X-rays is shown in Figure 6 below. The field of view of the XRT is 23.6 x 23.6 arc minutes and it has an angular resolution of 18 arc seconds. The XRT uses two timing modes to obtain light curves of the observed objects and resulting X-ray fluxes, window timing (WT) mode and photon counting (PC) mode. These modes are discussed in depth in Burrows et al. 2005.

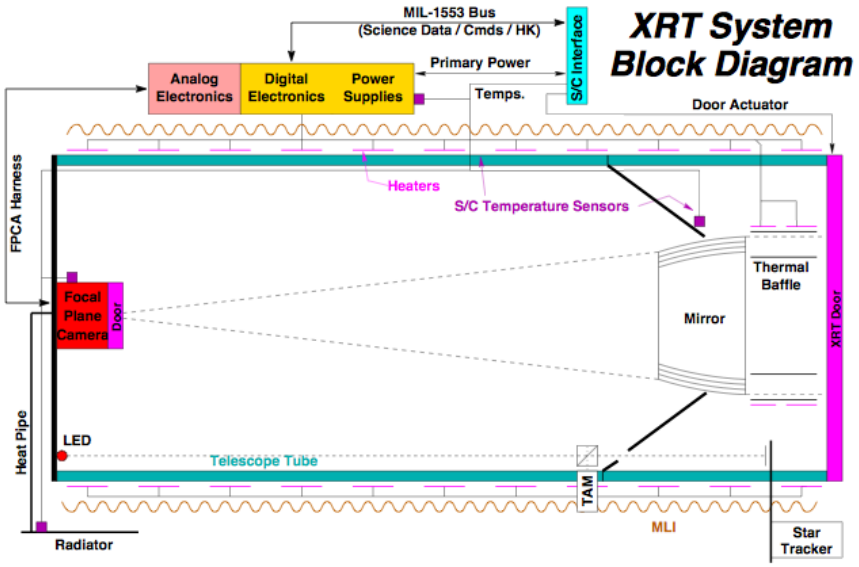


**Figure 6: Block diagram of the XRT that shows the X-ray photon path to the detector (Burrows et al., 2005).**

Since its launch the XRT has aided in the detection and identification of X-ray emitting objects throughout the universe. Due to its high sensitivity and the ability to monitor many of the *Fermi* objects throughout its mission, the *Swift*-XRT is the perfect instrument to utilize for our multi-wavelength X-ray analysis of the *Fermi* unassociated sources.

# Chapter 4

## The Data

The multivariate dataset was compiled using various public datasets and papers listing the X-ray and gamma-ray properties of the analyzed sources. The data were divided into three major categories: the known blazars and known pulsars that established the two training sets of data to be applied to our data mining methods and the list of unassociated 1FGL and 2FGL *Fermi* sources that established the test set of data. The blazar training set tested against the 1FGL excesses was compiled dependent on what sources in Third Catalog of Active Galactic Nuclei (3LAC; Ackermann et al., 2015) had a listed X-ray flux and additionally were listed in the 1FGL catalog. The blazar training set used to test against the 2FGL notable excesses was compiled dependent on what sources in the 3LAC catalog had a listed X-ray flux and additionally were listed in the 2FGL catalog. The pulsar training set was compiled by searching through the literature for follow up observations of known 1FGL or 2FGL pulsars that also had a determined X-ray flux. The *Fermi* unassociated test set was compiled by utilizing the *Swift*-XRT Survey of Unassociated *Fermi* Sources database (Stroh & Falcone 2013) available at http://www.swift.psu.edu/unassociated/. Our overall dataset that includes all the blazars, pulsars, and unassociated objects lists the observed X-ray flux dependent on the type of object as well as the following variables from the *Fermi* catalogs: Fermi name, gamma-ray flux greater than 1 GeV, spectral index, curvature index for 1FGL objects or curvature significance for 2FGL objects, and variability index. The tables that list all the properties can be found in Table 1 and Table 2. The specific data sets are discussed in more detail below.

## The Blazar Training Set

The 3LAC catalog is a comprehensive dataset of 1591 AGN detected by the *Fermi*-LAT and listed in the 3FGL catalog. The 3LAC catalog lists many multi-wavelength properties, when known, of the 3FGL sources, including X-ray flux in the 0.1-2.4 keV band. Of the 1591 AGN listed in the 3LAC catalog, 98% are blazars, thus making this dataset perfect for our analysis.

In compiling the blazar training set that we would use for our analysis we had to systematically check that an X-ray flux was known for the listed 3FGL object in the 3LAC catalog and that the object was also observed in the 1FGL or 2FGL catalog so that we can apply the proper analysis to our list of unassociated sources, which is discussed in the Analysis chapter. After applying these systematic checks, our blazar training set consists of 401 known blazars observed in the 1FGL catalog and 518 known blazars observed in the 2FGL catalog.

## The Pulsar Training Set

In compiling the pulsar training set we performed a literature search looking for known pulsars that are in the 1FGL or 2FGL catalog and also have a known X-ray flux. We found 20 pulsars in total that matched our criteria and compiled these sources as our pulsar training set. The specific pulsars that make up our training set include: 1FGL J0106.7+4853, 1FGL J1312.6+0048, 1FGL J2043.2+1709a, 1FGL J2043+1709b, and 1FGL J2302.8+4443 (Takahashi et al., 2012); 1FGL J0614.1-3328, 1FGL J1231.1-1410, and 1FGL J2214.8+3002 (Ransom et al., 2011); 1FGL J2017.3+0603 (Cognard et al., 2011); 1FGL J0622.2+3751, 1FGL J1620.8–4928c,

1FGL J1746.7–3233, 1FGL J1803.1–2147c, 1FGL J2030.9+4411, 1FGL J2111.3+4607, and 1FGL J2139.9+4715 (Pletsch et al., 2012); 1FGL J2030.0+3641 (Camilo et al., 2012); 1FGL J0101.0-6423 (Kerr et al., 2012); 1FGL J1311.7-3429 (Kataoka et al., 2012); 1FGL J1653.6-0158 (Romani et al., 2014).

The authors for each of the pulsar papers reported the determined X-ray fluxes of each of the pulsars in bands other that the 0.1-2.4 keV band used by the 3LAC catalog. The Ransom et al., Cognard et al., Camilo et al., Kerr et al., Kataoka et al., and Romani et al. papers all reported their X-ray fluxes in the 0.5-8.0 keV band. The Takahashi et al. paper reported the X-ray flux in the 2-10 keV band and the Pletsch et al. reported the X-ray flux in the 0.3-10.0 keV band. Therefore, in order to perform a proper comparison of the X-ray fluxes for our entire dataset we had to convert the fluxes from the reported bands to the 0.1-2.4 keV band.

The conversion of X-ray flux from the reported energy band to the 0.1-2.4 keV band was performed by utilizing PIMMS version 4.7d (Mukai 1993), which is available through NASA's HEASARC tools. PIMMS allows its users to convert known flux or count rates in many telescopes to source flux. In order to do the best possible conversion from the reported X-ray band to the 0.1-2.4 keV band we had to input a model parameter to PIMMS in addition to the neutral Hydrogen column density towards the observed pulsar. Some authors did not report a model parameter or an observed column density. When a model parameter was not reported, a power law model was assumed with a photon index of 2.0. If the galactic nH was also not reported we utilized the nH Column Density tool that was also available through NASA's HEASARC tools in order to approximate the galactic nH towards the observed pulsar. In our flux conversion we used the "Weighted average nH" reported by the LAB Survey of Galactic HI (Kalberla et al., 2005) of the nH Column Density HEASARC tool.

## The Unassociated Test Set

The unassociated test set consists of unassociated 1FGL and 2FGL objects that were also observed with the *Swift*-XRT and made publically available on the *Swift*-XRT survey of *Fermi* unassociated sources (Stroh & Falcone, 2013). The unassociated sources were split into two separate datasets: 1FGL notable excesses and 2FGL notable excesses. A notable excess was defined as a source detected by *Swift* that was within the 95% *Fermi* position confidence region of an unassociated *Fermi* source and had a signal to noise (SNR) ratio greater than 4.0. For the 1FGL objects, there was also an additional constraint of excesses being at least 5° from the galactic plane. Our unassociated test set consists of 191 total objects with 125 1FGL notable excesses and 66 2FGL notable excesses. There are 83 unique 1FGL unassociated objects amongst the 1FGL notable excesses and 53 unique 2FGL unassociated objects amongst 2FGL notable excesses. The reason that not all of 1FGL and 2FGL notable excesses are not unique *Fermi* unassociated sources is because there are sometimes multiple notable *Swift* excesses detected within a single *Fermi* field of view.

As with the pulsar data, the X-ray flux for the unassociated sources was not measured using the 0.1-2.4 keV band. The *Swift*-XRT instead measured a flux count rate in the 0.2-10.0 keV band. We therefore had to utilize the PIMMS tool again to obtain an approximated flux in the proper energy band. Neither spectral indices nor nH column density were known for the unassociated sources so we assumed a power law model with a spectral index of 2.0 and utilized the nH column density HEASARC tool to approximate the flux in the proper band. This approximation can obviously bring up some systematic errors within the analysis but we found that the errors with changing spectral index or column density to within reasonable amounts did not have a large impact on the approximated 0.1-2.4 keV X-ray flux. The 1FGL and 2FGL

notable excesses that comprised the test set of data, along with their properties are displayed below in Table 1 and Table 2.

**Table 1: 1FGL unassociated notable Swift excesses. X-ray flux units are in erg/cm$^2$/s in the 0.1-2.4 keV range. Gamma flux is flux greater than 1 GeV in units of photons/cm$^2$/s. Spectral index, curvature index, and variability index is that specified by Fermi. The SNR is the SOSTA value observed by Swift and available on the Swift unassociated site.**

| 1FGL Name | Swift Excess Name | X-ray Flux | Gamma Flux | Spectral Index | Curvature Index | Variability Index | SNR |
|---|---|---|---|---|---|---|---|
| J0001.9-4158 | J000132.8-415522 | 2.17E-12 | 5.26E-10 | 1.9227 | 4.232092 | 8.765109 | 18.780 |
| J0003.1+6227 | J000340.2+622526 | 4.90E-13 | 2.14E-09 | 2.5273 | 19.4988 | 15.191000 | 5.927 |
| J0009.1+5031 | J000922.4+503031 | 4.52E-13 | 1.28E-09 | 2.4103 | 1.330319 | 12.629790 | 5.411 |
| J0131.2+6121 | J013106.8+612035 | 1.21E-11 | 3.58E-09 | 2.2681 | 4.012742 | 7.205684 | 19.120 |
| J0137.8+5814 | J013750.3+581411 | 1.39E-11 | 1.43E-09 | 2.3940 | 4.08378 | 5.172387 | 27.220 |
| J0143.9-5845 | J014347.4-584552 | 1.67E-11 | 1.15E-09 | 1.9502 | 3.03556 | 5.867749 | 43.730 |
| J0212.3+5319 | J021210.5+532136 | 1.02E-12 | 2.49E-09 | 2.3862 | 4.527422 | 14.915820 | 8.437 |
| J0223.0-1118 | J022314.3-111739 | 1.35E-12 | 8.68E-10 | 1.5143 | 0.3739 | 5.102208 | 12.160 |
| J0316.3-6438 | J031614.1-643730 | 5.77E-12 | 6.74E-10 | 2.0332 | 0.5256731 | 6.205753 | 32.720 |
| J0335.5-4501 | J033513.7-445943 | 4.22E-13 | 6.89E-10 | 2.1224 | 4.373764 | 7.863986 | 6.934 |
| J0409.9-0357 | J040946.6-040000 | 2.73E-13 | 7.32E-10 | 2.1886 | 1.238775 | 12.140630 | 5.132 |
| J0430.3+3511c | J043041.1+351353 | 2.01E-12 | 1.28E-09 | 2.5166 | 7.365446 | 11.928750 | 10.790 |
| J0430.3+3511c | J043000.9+351723 | 1.42E-12 | 1.28E-09 | 2.5166 | 7.365446 | 11.928750 | 8.899 |
| J0430.3+3511c | J043019.3+351744 | 6.62E-13 | 1.28E-09 | 2.5166 | 7.365446 | 11.928750 | 5.954 |
| J0430.3+3511c | J043013.7+351339 | 5.36E-13 | 1.28E-09 | 2.5166 | 7.365446 | 11.928750 | 4.469 |
| J0430.3+3511c | J043103.5+350915 | 3.52E-13 | 1.28E-09 | 2.5166 | 7.365446 | 11.928750 | 4.272 |
| J0521.6+0103 | J052141.2+010251 | 9.53E-14 | 6.37E-10 | 2.1135 | 1.778347 | 7.543861 | 5.343 |
| J0521.6+0103 | J052153.10+005936 | 8.91E-14 | 6.37E-10 | 2.1135 | 1.778347 | 7.543861 | 5.182 |
| J0521.6+0103 | J052203.0+010552 | 8.22E-14 | 6.37E-10 | 2.1135 | 1.778347 | 7.543861 | 5.117 |
| J0523.5-2529 | J052316.5-252737 | 1.37E-13 | 2.61E-09 | 2.2121 | 12.06014 | 10.288270 | 6.006 |
| J0523.5-2529 | J052323.9-252731 | 8.78E-14 | 2.61E-09 | 2.2121 | 12.06014 | 10.288270 | 4.777 |
| J0534.7-0531c | J053456.5-053136 | 1.86E-12 | 2.98E-09 | 2.3671 | 12.99037 | 4.604013 | 10.850 |
| J0534.7-0531c | J053427.7-053154 | 9.29E-13 | 2.98E-09 | 2.3671 | 12.99037 | 4.604013 | 7.852 |
| J0534.7-0531c | J053434.0-052821 | 9.14E-13 | 2.98E-09 | 2.3671 | 12.99037 | 4.604013 | 7.743 |
| J0534.7-0531c | J053503.5-052952 | 6.70E-13 | 2.98E-09 | 2.3671 | 12.99037 | 4.604013 | 6.372 |
| J0534.7-0531c | J053440.1-052642 | 6.00E-13 | 2.98E-09 | 2.3671 | 12.99037 | 4.604013 | 6.119 |
| J0534.7-0531c | J053455.8-052916 | 5.11E-13 | 2.98E-09 | 2.3671 | 12.99037 | 4.604013 | 5.333 |
| J0534.7-0531c | J053435.2-053210 | 4.31E-13 | 2.98E-09 | 2.3671 | 12.99037 | 4.604013 | 5.074 |
| J0536.2-0607c | J053631.4-060826 | 4.53E-13 | 2.32E-09 | 2.3409 | 6.082151 | 3.350236 | 4.641 |
| J0536.2-0607c | J053622.3-060228 | 3.71E-13 | 2.32E-09 | 2.3409 | 6.082151 | 3.350236 | 4.209 |
| J0605.3+3800 | J060503.5+375738 | 3.64E-13 | 1.26E-09 | 1.9899 | 3.216397 | 4.518563 | 4.518 |

| 1FGL Name | Swift Excess Name | X-ray Flux | Gamma Flux | Spectral Index | Curvature Index | Variability Index | SNR |
|---|---|---|---|---|---|---|---|
| J0648.8+1516 | J064847.6+151623 | 2.00E-11 | 1.76E-09 | 1.8074 | 1.088437 | 7.142142 | 59.980 |
| J0659.9+1303 | J070014.3+130423 | 8.35E-13 | 6.00E-10 | 2.1063 | 2.183354 | 3.653571 | 7.631 |
| J0734.7-1557 | J073437.6-155612 | 1.06E-12 | 3.95E-09 | 2.3943 | 14.70003 | 6.582773 | 8.687 |
| J0744.1-2523 | J074346.6-252510 | 1.08E-13 | 3.01E-09 | 2.3123 | 10.97605 | 9.339464 | 4.031 |
| J0746.5-0711 | J074639.8-071716 | 2.78E-13 | 8.69E-10 | 2.1439 | 2.766893 | 7.819942 | 4.149 |
| J0823.3-4248 | J082324.7-425012 | 1.55E-11 | 6.90E-09 | 1.9986 | 32.05555 | 12.345980 | 21.450 |
| J0823.3-4248 | J082334.3-424631 | 7.80E-12 | 6.90E-09 | 1.9986 | 32.05555 | 12.345980 | 12.040 |
| J0823.3-4248 | J082336.1-424717 | 5.97E-12 | 6.90E-09 | 1.9986 | 32.05555 | 12.345980 | 9.604 |
| J0823.3-4248 | J082328.10-425136 | 4.69E-12 | 6.90E-09 | 1.9986 | 32.05555 | 12.345980 | 7.954 |
| J0823.3-4248 | J082341.1-425050 | 4.82E-12 | 6.90E-09 | 1.9986 | 32.05555 | 12.345980 | 7.705 |
| J0823.3-4248 | J082328.1-424354 | 3.36E-12 | 6.90E-09 | 1.9986 | 32.05555 | 12.345980 | 7.531 |
| J0823.3-4248 | J082304.7-425214 | 3.58E-12 | 6.90E-09 | 1.9986 | 32.05555 | 12.345980 | 7.332 |
| J0823.3-4248 | J082310.1-425001 | 3.81E-12 | 6.90E-09 | 1.9986 | 32.05555 | 12.345980 | 7.330 |
| J0823.3-4248 | J082317.9-424933 | 3.63E-12 | 6.90E-09 | 1.9986 | 32.05555 | 12.345980 | 5.871 |
| J0838.6-2828 | J083843.4-282701 | 4.35E-12 | 1.22E-09 | 2.1213 | 8.053023 | 12.022430 | 36.310 |
| J0841.4-3558 | J084121.7-355507 | 9.41E-12 | 1.31E-09 | 1.7620 | 1.197991 | 10.546810 | 21.780 |
| J0841.4-3558 | J084121.3-355715 | 4.16E-12 | 1.31E-09 | 1.7620 | 1.197991 | 10.546810 | 13.190 |
| J0848.6+0504 | J084839.6+050620 | 1.85E-12 | 7.57E-10 | 1.2406 | 0.5186078 | 1.871207 | 13.350 |
| J0849.4-2912 | J084900.10-291149 | 3.59E-13 | 8.61E-10 | 2.0753 | 1.418967 | 7.611750 | 5.194 |
| J0908.7-2119 | J090858.6-211852 | 1.32E-12 | 8.30E-10 | 2.1991 | 12.73658 | 4.541736 | 9.329 |
| J0922.0+2337 | J092145.2+233547 | 2.20E-13 | 9.33E-10 | 1.6620 | 0.8194752 | 2.148683 | 4.606 |
| J1033.5-5033 | J103332.4-503526 | 1.77E-12 | 1.02E-09 | 1.5248 | 0.792316 | 4.889848 | 10.400 |
| J1040.5+0616 | J104031.7+061722 | 2.87E-13 | 1.32E-09 | 2.5618 | 2.921882 | 24.957610 | 9.050 |
| J1040.5+0616 | J104039.4+061523 | 1.67E-13 | 1.32E-09 | 2.5618 | 2.921882 | 24.957610 | 7.175 |
| J1040.5+0616 | J104048.4+061821 | 7.85E-14 | 1.32E-09 | 2.5618 | 2.921882 | 24.957610 | 4.691 |
| J1040.9-1205 | J104108.6-120330 | 4.79E-13 | 8.48E-10 | 2.1653 | 0.6950651 | 5.272589 | 6.461 |
| J1040.9-1205 | J104048.6-120618 | 2.14E-13 | 8.48E-10 | 2.1653 | 0.6950651 | 5.272589 | 4.346 |
| J1110.3-1622 | J111017.10-162401 | 2.75E-13 | 6.70E-10 | 1.9756 | 1.229654 | 3.115109 | 4.428 |
| J1115.2-6124c | J111453.3-612421 | 4.35E-13 | 5.82E-09 | 2.2507 | 3.776485 | 9.343749 | 4.930 |
| J1117.0-5339 | J111715.2-533816 | 7.37E-13 | 9.05E-10 | 1.9453 | 0.7036873 | 6.679425 | 6.343 |
| J1119.9-2205 | J111959.1-220455 | 7.87E-14 | 3.04E-09 | 2.2400 | 16.85996 | 16.118970 | 8.688 |
| J1119.9-2205 | J111952.7-220637 | 5.99E-14 | 3.04E-09 | 2.2400 | 16.85996 | 16.118970 | 7.585 |
| J1119.9-2205 | J112010.2-220811 | 2.67E-14 | 3.04E-09 | 2.2400 | 16.85996 | 16.118970 | 4.707 |
| J1119.9-2205 | J112001.1-220130 | 2.53E-14 | 3.04E-09 | 2.2400 | 16.85996 | 16.118970 | 4.491 |
| J1123.6-4555 | J112355.5-455019 | 3.52E-13 | 8.88E-10 | 2.3650 | 1.708008 | 6.486578 | 5.013 |
| J1141.8-1403 | J114141.7-140755 | 2.54E-12 | 6.70E-10 | 2.0815 | 0.9335002 | 5.835430 | 19.660 |
| J1221.4-0635 | J122127.2-062847 | 2.64E-13 | 9.04E-10 | 2.6166 | 1.746582 | 11.876750 | 9.401 |

| 1FGL Name | Swift Excess Name | X-ray Flux | Gamma Flux | Spectral Index | Curvature Index | Variability Index | SNR |
|---|---|---|---|---|---|---|---|
| J1223.4-3034 | J122336.9-303250 | 2.93E-12 | 1.27E-09 | 2.2164 | 2.88252 | 2.992682 | 11.510 |
| J1226.0+2954 | J122608.3+295942 | 2.69E-13 | 1.18E-09 | 2.0544 | 4.342566 | 7.076197 | 4.910 |
| J1227.9-4852 | J122758.7-485342 | 8.00E-12 | 3.41E-09 | 2.4468 | 8.41156 | 3.753376 | 93.010 |
| J1227.9-4852 | J122724.8-485555 | 7.48E-14 | 3.41E-09 | 2.4468 | 8.41156 | 3.753376 | 7.979 |
| J1227.9-4852 | J122742.9-485225 | 3.95E-14 | 3.41E-09 | 2.4468 | 8.41156 | 3.753376 | 4.958 |
| J1227.9-4852 | J122823.1-485038 | 3.44E-14 | 3.41E-09 | 2.4468 | 8.41156 | 3.753376 | 4.809 |
| J1240.3-7154 | J124021.4-714858 | 1.42E-11 | 1.56E-09 | 2.2795 | 3.412898 | 8.134727 | 34.810 |
| J1249.3-2812 | J124919.4-280832 | 1.71E-12 | 7.88E-10 | 1.6434 | 0.5035008 | 3.491324 | 12.260 |
| J1250.9-4940 | J125058.8-494447 | 2.84E-13 | 1.05E-09 | 2.2454 | 3.955786 | 8.345318 | 4.558 |
| J1256.1-5922 | J125605.9-591941 | 3.59E-13 | 1.33E-09 | 2.2175 | 2.418205 | 3.898082 | 4.340 |
| J1258.3+2125 | J125821.5+212351 | 6.07E-13 | 6.50E-10 | 1.2970 | 0.4770743 | 1.136436 | 7.691 |
| J1306.4-6038 | J130601.9-603358 | 5.75E-13 | 4.22E-09 | 2.2532 | 13.23737 | 14.388900 | 5.658 |
| J1322.1+0838 | J132210.2+084231 | 4.31E-13 | 6.35E-10 | 2.0882 | 3.180147 | 14.238570 | 8.811 |
| J1322.1+0838 | J132222.9+084320 | 1.09E-13 | 6.35E-10 | 2.0882 | 3.180147 | 14.238570 | 4.028 |
| J1340.5-0413 | J134042.1-041008 | 7.45E-13 | 8.87E-10 | 1.8102 | 3.774195 | 10.481030 | 11.150 |
| J1353.6-6640 | J135339.10-664000 | 6.71E-12 | 1.52E-09 | 2.3373 | 2.657531 | 4.244449 | 16.530 |
| J1412.6+7406 | J141234.9+741158 | 2.03E-13 | 5.42E-10 | 2.7086 | 3.901942 | 10.419220 | 5.634 |
| J1419.7+7731 | J141901.2+773228 | 2.75E-12 | 5.03E-10 | 1.8785 | 0.6651357 | 6.101304 | 16.920 |
| J1446.8-4702 | J144719.8-470102 | 1.12E-13 | 1.72E-09 | 2.4204 | 5.033468 | 3.565653 | 4.082 |
| J1511.8-0513 | J151148.6-051347 | 1.79E-11 | 1.42E-09 | 2.3049 | 1.889656 | 10.224640 | 39.470 |
| J1511.8-0513 | J151200.1-051528 | 3.14E-13 | 1.42E-09 | 2.3049 | 1.889656 | 10.224640 | 4.885 |
| J1511.9-2253 | J151212.8-225506 | 1.03E-12 | 6.98E-10 | 2.1743 | 3.453869 | 2.638998 | 9.191 |
| J1511.9-2253 | J151137.1-225744 | 3.94E-13 | 6.98E-10 | 2.1743 | 3.453869 | 2.638998 | 5.283 |
| J1539.0-3328 | J153924.7-332839 | 6.51E-14 | 3.58E-09 | 1.8901 | 28.07603 | 10.547450 | 7.806 |
| J1539.0-3328 | J153900.6-332702 | 2.56E-14 | 3.58E-09 | 1.8901 | 28.07603 | 10.547450 | 4.312 |
| J1549.7-0659 | J154952.1-065908 | 4.69E-12 | 1.46E-09 | 2.2374 | 3.467695 | 3.727824 | 18.670 |
| J1625.8-2429c | J162558.1-243029 | 6.41E-13 | 4.90E-09 | 2.2534 | 11.08445 | 4.213712 | 5.491 |
| J1639.5-5152 | J163926.3-514933 | 5.73E-13 | 3.95E-09 | 2.5392 | 9.040545 | 14.351910 | 6.392 |
| J1650.3-5410 | J165043.10-540508 | 3.79E-13 | 1.14E-09 | 2.2396 | 5.644106 | 9.675350 | 4.160 |
| J1656.2-3257 | J165616.9-330211 | 4.79E-12 | 2.06E-09 | 2.4374 | 2.936643 | 41.435230 | 25.320 |
| J1656.2-3257 | J165557.8-325946 | 4.28E-13 | 2.06E-09 | 2.4374 | 2.936643 | 41.435230 | 7.359 |
| J1816.7+4509 | J181652.5+450731 | 2.00E-13 | 1.58E-09 | 2.3309 | 1.358856 | 10.061160 | 4.524 |
| J1823.5-3454 | J182338.8-345412 | 2.85E-11 | 1.78E-09 | 1.7007 | 3.009613 | 9.277560 | 43.260 |
| J1831.5-0200c | J183126.7-020518 | 1.91E-12 | 7.20E-09 | 2.5194 | 16.73256 | 17.535420 | 12.250 |
| J1831.5-0200c | J183113.5-020350 | 2.26E-13 | 7.20E-09 | 2.5194 | 16.73256 | 17.535420 | 4.034 |
| J1835.3+1345 | J183539.5+135048 | 3.20E-13 | 7.90E-10 | 2.3444 | 2.996214 | 7.119668 | 4.190 |
| J1842.3-5845 | J184229.10-584158 | 1.13E-11 | 5.89E-10 | 1.7043 | 5.05528 | 6.831230 | 39.070 |

| 1FGL Name | Swift Excess Name | X-ray Flux | Gamma Flux | Spectral Index | Curvature Index | Variability Index | SNR |
|---|---|---|---|---|---|---|---|
| J1844.1+1547 | J184425.4+154643 | 4.06E-12 | 1.56E-09 | 2.3413 | 6.301886 | 11.416170 | 15.000 |
| J1857.1+0212c | J185651.5+021023 | 2.35E-13 | 1.77E-08 | 2.3192 | 45.88687 | 8.791679 | 4.458 |
| J1933.3+0723 | J193320.2+072619 | 4.39E-12 | 9.87E-10 | 2.3183 | 3.152826 | 6.463311 | 15.380 |
| J1942.7+1033 | J194247.5+103327 | 9.38E-12 | 3.43E-09 | 1.7753 | 11.98504 | 8.322110 | 20.620 |
| J2004.8+7004 | J200505.5+700437 | 4.90E-12 | 1.88E-09 | 1.9417 | 3.879144 | 13.035120 | 20.900 |
| J2014.4+0647 | J201431.1+064850 | 1.85E-12 | 9.25E-10 | 1.7773 | 0.3476834 | 4.990013 | 25.090 |
| J2014.4+0647 | J201410.9+064354 | 1.22E-13 | 9.25E-10 | 1.7773 | 0.3476834 | 4.990013 | 5.778 |
| J2034.6-4202 | J203450.8-420038 | 1.44E-12 | 9.93E-10 | 1.9636 | 2.338899 | 5.708535 | 12.180 |
| J2037.0-3329 | J203649.6-332829 | 3.78E-12 | 9.09E-10 | 2.0153 | 2.70337 | 4.534122 | 22.860 |
| J2043.2+1709 | J204312.9+171019 | 1.53E-13 | 4.51E-09 | 2.1287 | 12.03429 | 12.221580 | 5.464 |
| J2043.2+1709 | J204318.7+170755 | 1.46E-13 | 4.51E-09 | 2.1287 | 12.03429 | 12.221580 | 5.083 |
| J2056.7+4938 | J205642.7+494008 | 2.89E-11 | 1.67E-09 | 1.8516 | 1.676268 | 4.354281 | 49.790 |
| J2058.8-3903 | J205902.5-385936 | 2.06E-13 | 1.00E-09 | 1.6708 | 0.6766586 | 3.665547 | 4.269 |
| J2104.6+2119 | J210415.9+211807 | 6.39E-13 | 9.81E-10 | 2.1994 | 1.673621 | 9.020142 | 6.549 |
| J2107.5+5202c | J210720.4+520257 | 1.62E-12 | 3.24E-09 | 2.5356 | 25.69457 | 8.560507 | 6.900 |
| J2129.8-0427 | J213008.1-043452 | 3.03E-13 | 1.05E-09 | 2.3299 | 2.124532 | 9.928521 | 8.100 |
| J2129.8-0427 | J212945.4-042910 | 1.45E-13 | 1.05E-09 | 2.3299 | 2.124532 | 9.928521 | 5.589 |
| J2216.1+5139 | J221545.9+514454 | 1.26E-13 | 1.99E-09 | 2.2642 | 6.12102 | 9.148273 | 4.662 |
| J2257.9-3643 | J225756.10-364607 | 1.92E-13 | 8.91E-10 | 2.0706 | 5.410129 | 2.329847 | 4.105 |
| J2257.9-3643 | J225814.8-364430 | 1.81E-13 | 8.91E-10 | 2.0706 | 5.410129 | 2.329847 | 4.078 |

**Table 2: 2FGL unassociated notable Swift excesses. X-ray flux units are in erg/cm$^2$/s in the 0.1-2.4 keV range. Gamma flux is flux greater than 1 GeV in units of photons/cm$^2$/s. Spectral index, curvature significance, and variability index is that specified by Fermi. The SNR is the SOSTA value observed by Swift and available on the Swift unassociated site.**

| 2FGL Name | Swift Excess Name | X-ray Flux | Gamma Flux | Spectral Index | Curvature Signif. | Variability Index | SNR |
|---|---|---|---|---|---|---|---|
| J0031.0+0724 | J003119.7+072451 | 2.66E-13 | 3.48E-10 | 1.8948 | 0.83 | 20.88069 | 11.64 |
| J0031.0+0724 | J003054.7+072325 | 3.26E-14 | 3.48E-10 | 1.8948 | 0.83 | 20.88069 | 4.019 |
| J0048.8-6347 | J004935.8-634745 | 4.98E-13 | 3.51E-10 | 2.0452 | 2.12 | 23.32265 | 8.674 |
| J0116.6-6153 | J011619.2-615341 | 1.62E-13 | 3.10E-10 | 1.6335 | 0.48 | 23.92089 | 4.232 |
| J0133.4-4408 | J013321.6-441314 | 1.50E-13 | 4.47E-10 | 2.0699 | 0.53 | 22.42753 | 5.056 |
| J0200.4-4105 | J020020.8-410933 | 3.46E-13 | 3.33E-10 | 1.8179 | 0.08 | 30.03589 | 7.923 |
| J0222.7+6820 | J022302.8+682157 | 4.94E-13 | 7.54E-10 | 2.1342 | 0.02 | 18.95654 | 10.45 |
| J0226.1+0943 | J022613.6+093723 | 6.80E-14 | 6.84E-10 | 2.1024 | 0.47 | 49.67666 | 5.062 |
| J0338.2+1306 | J033829.3+130215 | 9.49E-13 | 5.86E-10 | 1.5354 | 1.9 | 35.91702 | 15.17 |
| J0353.2+5653 | J035309.5+565428 | 3.45E-13 | 8.42E-10 | 2.1126 | 0.98 | 29.73964 | 8.963 |
| J0438.0-7331 | J043836.9-732920 | 1.62E-13 | 3.99E-10 | 1.4446 | 0.71 | 30.11527 | 5.092 |
| J0458.4+0654 | J045802.6+065012 | 3.47E-13 | 6.11E-10 | 2.4376 | 0.27 | 39.74677 | 9.239 |

| 2FGL Name | Swift Excess Name | X-ray Flux | Gamma Flux | Spectral Index | Curvature Signif. | Variability Index | SNR |
|---|---|---|---|---|---|---|---|
| J0529.3+3821 | J052939.4+382323 | 1.12E-13 | 1.00E-09 | 2.0907 | 3.06 | 20.80639 | 5.195 |
| J0644.6+6034 | J064436.1+603852 | 3.68E-13 | 8.94E-10 | 2.1073 | 0.32 | 32.19475 | 6.184 |
| J0658.4+0633 | J065845.2+063711 | 1.52E-13 | 6.56E-10 | 2.3129 | 1.36 | 17.65983 | 5.518 |
| J0725.8-0549 | J072547.5-054830 | 7.22E-13 | 4.20E-10 | 1.7751 | 0.44 | 25.39904 | 10.99 |
| J0737.1-3235 | J073713.10-323627 | 1.01E-13 | 1.33E-09 | 2.3341 | 3.14 | 50.94962 | 5.397 |
| J0737.1-3235 | J073738.9-323257 | 5.66E-14 | 1.33E-09 | 2.3341 | 3.14 | 50.94962 | 4.064 |
| J0737.5-8246 | J073705.0-824842 | 3.91E-13 | 2.80E-10 | 1.3492 | 1.76 | 19.56135 | 11.48 |
| J0737.5-8246 | J073820.2-825042 | 2.06E-13 | 2.80E-10 | 1.3492 | 1.76 | 19.56135 | 8.021 |
| J0745.5+7910 | J074513.0+791315 | 1.07E-13 | 4.08E-10 | 2.2291 | 2.37 | 29.28214 | 5.61 |
| J0802.6-0940 | J080215.9-094214 | 3.49E-13 | 5.23E-10 | 1.9677 | 0.11 | 21.431 | 7.374 |
| J0846.7-4053 | J084722.5-404736 | 8.86E-13 | 1.39E-09 | 2.476 | 3.27 | 41.46843 | 14.85 |
| J0846.7-4053 | J084636.5-410300 | 1.06E-13 | 1.39E-09 | 2.476 | 3.27 | 41.46843 | 4.736 |
| J0859.4-2532 | J085929.8-253107 | 5.39E-13 | 5.89E-10 | 2.064 | 0.05 | 26.9303 | 7.324 |
| J0900.9+6736 | J090121.6+673956 | 1.26E-13 | 4.85E-10 | 2.4664 | 1.33 | 34.96169 | 7.55 |
| J0900.9+6736 | J090110.4+674203 | 1.05E-13 | 4.85E-10 | 2.4664 | 1.33 | 34.96169 | 7.069 |
| J0900.9+6736 | J090015.5+673809 | 4.46E-14 | 4.85E-10 | 2.4664 | 1.33 | 34.96169 | 4.549 |
| J0937.9-1434 | J093754.6-143349 | 1.73E-13 | 3.99E-10 | 1.8932 | 0.98 | 15.4904 | 5.053 |
| J0937.9-1434 | J093738.2-142930 | 1.61E-13 | 3.99E-10 | 1.8932 | 0.98 | 15.4904 | 4.792 |
| J1013.6+3434 | J101351.5+343418 | 1.24E-13 | 3.48E-10 | 2.0919 | 1.57 | 22.42701 | 4.252 |
| J1016.4-4244 | J101620.7-424722 | 3.65E-13 | 5.54E-10 | 1.8092 | 1.24 | 32.49113 | 9.36 |
| J1016.4-4244 | J101635.5-424322 | 1.15E-13 | 5.54E-10 | 1.8092 | 1.24 | 32.49113 | 4.889 |
| J1029.5-2022 | J102946.8-201813 | 1.11E-13 | 4.56E-10 | 1.9994 | 0.38 | 25.86252 | 4.002 |
| J1038.2-2423 | J103755.0-242545 | 2.01E-13 | 5.95E-10 | 2.3093 | 0.84 | 19.32109 | 5.455 |
| J1038.2-2423 | J103748.3-242847 | 1.34E-13 | 5.95E-10 | 2.3093 | 0.84 | 19.32109 | 4.348 |
| J1056.2-6021 | J105645.1-601939 | 1.63E-14 | 6.10E-09 | 2.4691 | 5.36 | 34.51778 | 4.402 |
| J1058.7-6621 | J105832.1-662603 | 2.15E-13 | 9.55E-10 | 2.2306 | 0.32 | 16.63366 | 6.092 |
| J1105.4-7622 | J110451.2-762542 | 4.04E-13 | 7.11E-10 | 2.4344 | 0.71 | 16.4861 | 7.872 |
| J1105.4-7622 | J110409.3-762723 | 3.03E-13 | 7.11E-10 | 2.4344 | 0.71 | 16.4861 | 6.728 |
| J1105.4-7622 | J110552.1-761830 | 2.90E-13 | 7.11E-10 | 2.4344 | 0.71 | 16.4861 | 6.425 |
| J1105.6-6114 | J110506.4-611602 | 3.25E-14 | 4.98E-09 | 2.7139 | 6.4 | 18.45534 | 4.704 |
| J1105.6-6114 | J110619.3-611419 | 2.62E-14 | 4.98E-09 | 2.7139 | 6.4 | 18.45534 | 4.27 |
| J1259.8-3749 | J125949.7-374856 | 1.76E-13 | 6.38E-10 | 1.9097 | 0.1 | 32.74953 | 4.961 |
| J1317.2-6304 | J131710.7-630211 | 4.23E-14 | 5.43E-09 | 2.4275 | 5.63 | 19.03477 | 4.394 |
| J1347.0-2956 | J134706.8-295842 | 7.48E-13 | 3.57E-10 | 1.3576 | 0.19 | 21.80749 | 10.05 |
| J1347.0-2956 | J134702.8-295216 | 2.02E-13 | 3.57E-10 | 1.3576 | 0.19 | 21.80749 | 4.528 |
| J1424.2-1752 | J142412.5-175008 | 5.86E-13 | 7.18E-10 | 1.9737 | 0.47 | 23.35734 | 11.93 |
| J1502.1+5548 | J150217.7+554512 | 1.71E-13 | 4.33E-10 | 2.6451 | 0.87 | 46.61092 | 4.194 |
| J1617.3-5336 | J161646.7-534340 | 1.30E-13 | 1.41E-09 | 2.5362 | 3.63 | 19.33995 | 4.917 |
| J1659.2-0142 | J165922.2-014110 | 1.45E-13 | 9.63E-10 | 2.0464 | 0.92 | 27.81754 | 4.318 |

| 2FGL Name | Swift Excess Name | X-ray Flux | Gamma Flux | Spectral Index | Curvature Signif. | Variability Index | SNR |
|---|---|---|---|---|---|---|---|
| J1704.3+1235 | J170409.6+123423 | 1.52E-12 | 5.87E-10 | 2.1864 | 0.42 | 18.42241 | 18.07 |
| J1704.6-0529 | J170433.9-052840 | 1.33E-12 | 1.36E-09 | 2.3498 | 1.85 | 19.92329 | 19.05 |
| J1726.6-3545 | J172641.8-354053 | 3.16E-13 | 4.40E-09 | 2.4415 | 6.76 | 29.53417 | 9.534 |
| J1813.6-2821 | J181357.8-282043 | 1.32E-13 | 9.69E-10 | 2.4276 | 0.99 | 23.43587 | 4.433 |
| J1828.7+3231 | J182915.5+323432 | 2.60E-13 | 6.60E-10 | 2.2357 | 3.03 | 20.5236 | 6.918 |
| J1842.3-5839 | J184230.0-584158 | 5.16E-12 | 6.08E-10 | 1.7896 | 0.59 | 20.16694 | 39.89 |
| J1904.8-0705 | J190444.5-070743 | 1.76E-13 | 1.92E-09 | 2.4793 | 3.08 | 22.32177 | 5.138 |
| J1908.8-0132 | J190843.4-012954 | 8.42E-14 | 1.37E-09 | 2.5998 | 1.21 | 22.71176 | 5.14 |
| J1924.9-1036 | J192501.5-104317 | 1.83E-13 | 1.48E-09 | 2.2707 | 2.26 | 14.45801 | 5.154 |
| J2115.4+1213 | J211522.1+121801 | 1.59E-13 | 5.21E-10 | 2.3795 | 1.47 | 25.30516 | 4.742 |
| J2133.5-6431 | J213311.2-643819 | 2.65E-13 | 7.08E-10 | 2.2978 | 3.92 | 15.35901 | 9.061 |
| J2237.2+6316 | J223704.3+632336 | 8.06E-14 | 1.36E-09 | 2.3917 | 1.32 | 16.82248 | 9.225 |
| J2237.2+6316 | J223646.1+631605 | 2.73E-14 | 1.36E-09 | 2.3917 | 1.32 | 16.82248 | 4.982 |
| J2249.1+5758 | J224907.5+580304 | 1.20E-13 | 1.10E-09 | 1.9907 | 2.16 | 14.71786 | 4.947 |
| J2351.6-7558 | J235115.10-760016 | 4.29E-13 | 4.01E-10 | 1.9153 | 2.19 | 20.84251 | 7.906 |

# Chapter 5 Analysis

The primary goal of the analysis was to see if there was any clear distinction between the measured variables in the blazar and pulsar training sets and then use the observed separations to systematically approximate associations for the unassociated test set of data. In particular, we were analyzing our data to show that the addition of X-ray flux to *Fermi* properties can provide much greater constraints on known training set variables to provide greater confidence in association of unassociated *Fermi* objects. The motivating plot behind this additional X-ray analysis can be seen in Figure 7.

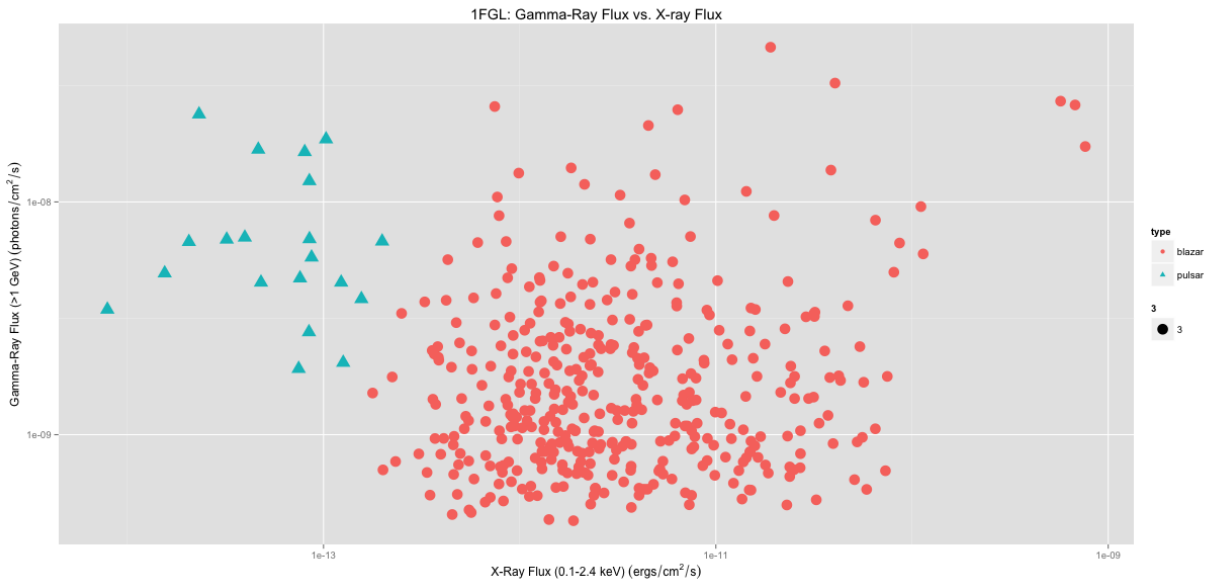


**Figure 7: Plot of gamma-ray flux versus X-ray flux of known pulsars and blazars. Blazars are labeled by red circles, pulsars are labeled by blue triangles.**

Figure 7, created through the use of the "ggplot2" package (Wickham, 2009) in R (R Core Team, 2014) as were similar plots in Appendix A and Appendix B, displays a clear separation in the X-ray flux versus gamma-ray properties for the training sets of the known

pulsars (blue triangles) and the known blazars (red circles). We used this information as motivation to compare the X-ray flux versus other gamma-ray properties, such as variability index, curvature index, and spectral index, made available by *Fermi* to systematically show distinctions in the pulsar and blazar training sets. This type of analysis has been done in the past with solely *Fermi* properties (Ackermann et al., 2012; Mirabal et al., 2012; Hassan et al., 2013; Doert et al., 2014) but it has never been attempted with additional X-ray properties added. From Figure 7 we can already see that our addition of X-ray flux will significantly aid in our distinction of the properties of known pulsars and blazars.

The next step of the analysis was to plot all the data in a similar fashion to Figure 7, while simultaneously over plotting the 1FGL and 2FGL test set properties to search for further separations. Once it was determined what properties created the most significant separations in the data we were able to utilize data mining techniques to approximate associations of the 1FGL and 2FGL notable excesses. These plots, with 1FGL and 2FGL test set points included can be seen in Figure 8 and Figure 9, which were created with the "GGally" CRAN package (Schloerke et al., 2014). Individual plots, before the association of the 1FGL and 2FGL notable excesses, of the pairs plots shown in Figure 8 and Figure 9 can be found in Appendix A. We attempted associations, in particular, through a k nearest neighbor (knn) test, performed using R. The variables that we utilized for our knn test include X-ray flux, gamma-ray flux, spectral index, and variability index for both 1FGL and 2FGL notable excesses. We additionally used the curvature index for the 1FGL excesses and the curvature significance for the 2FGL excesses. All of these variables are defined in the 1FGL (Abdo et al., 2010a) and 2FGL (Nolan et al., 2012) catalogs.

A knn test is a useful and easy to understand data mining technique that finds clear separations in training sets, when present. In performing a knn test the user will plot all known

variables in scaled parameter space and then determine the distances between the training data points with the test points to associated objects. In a simple knn test, the user will define a k value that stands for the number of training set points, or nearest neighbors, to be considered. The program will then determine the association for the test set point, based on the highest type of training set points closest to the test set. For example, if I assigned a k value of 5 for my knn test and my program found that for a particular test set point in parameter space that 3 of its closest neighbors were pulsars and 2 were blazars, then my test set point would be identified as a pulsar. The program will then perform a similar analysis for the remaining test set points and find associations for each object. More accurate knn tests can be performed by weighting the nearest neighbors dependent on how close they are to the test set point in parameter space and what "nearest neighbor" rank the training set point is. We implemented this type of knn test to our analysis to obtain stronger confidence in the results.

In our analysis we specifically used the "kknn" function in R provided by the "kknn" CRAN package (Schliep & Hechenbichler, 2014). The kknn function puts weight on the training set points considered; dependent on their distance from the test set point and their rank in distance from the test set point. The kknn function also attempts to provide probabilities on the association of test set points based on these weighted results. In our analysis we considered a k value of 6 nearest neighbors and scaled the properties appropriately by utilizing the scale feature in the kknn CRAN package.

It should be noted that there are some unavoidable issues associated with knn tests when associating objects. One issue can result from a specific parameter that has much more significance in separating the objects in parameter space, thus incorrectly associating objects. This is alleviated to some extent through scaling the variables as we have in our analysis. Issues

can also arise when dealing with sparse data. If our training sets consisted of only 2 pulsars and 100 blazars, for example, all test set points would be identified as blazars because there would always be at least 4 closest neighbors that were blazars for our chosen k value of 6. These issues must be considered when discussing results and trusting reported probabilities.

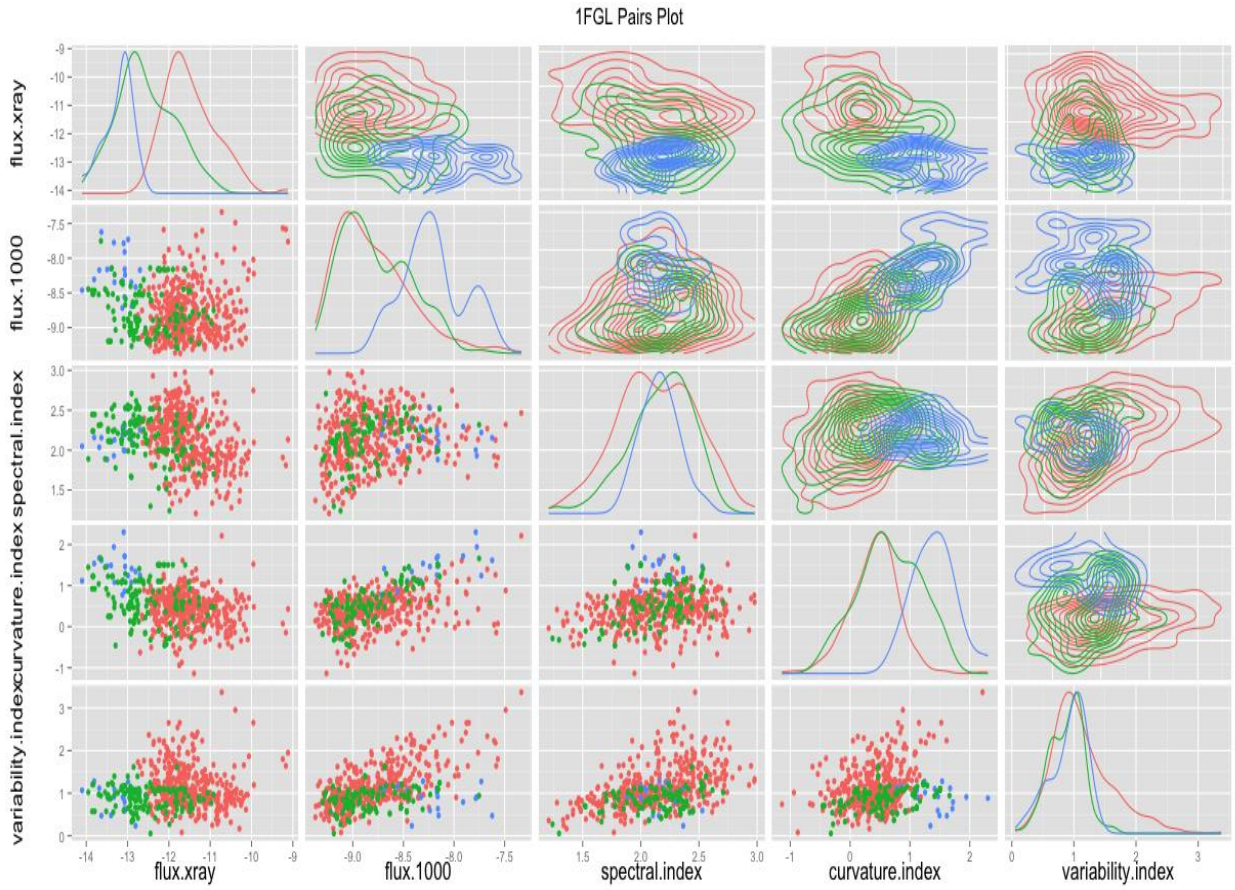


**Figure 8: Density plot of 1FGL data. Red points are known blazars, blue points are known pulsars, and green points are unassociated objects.**

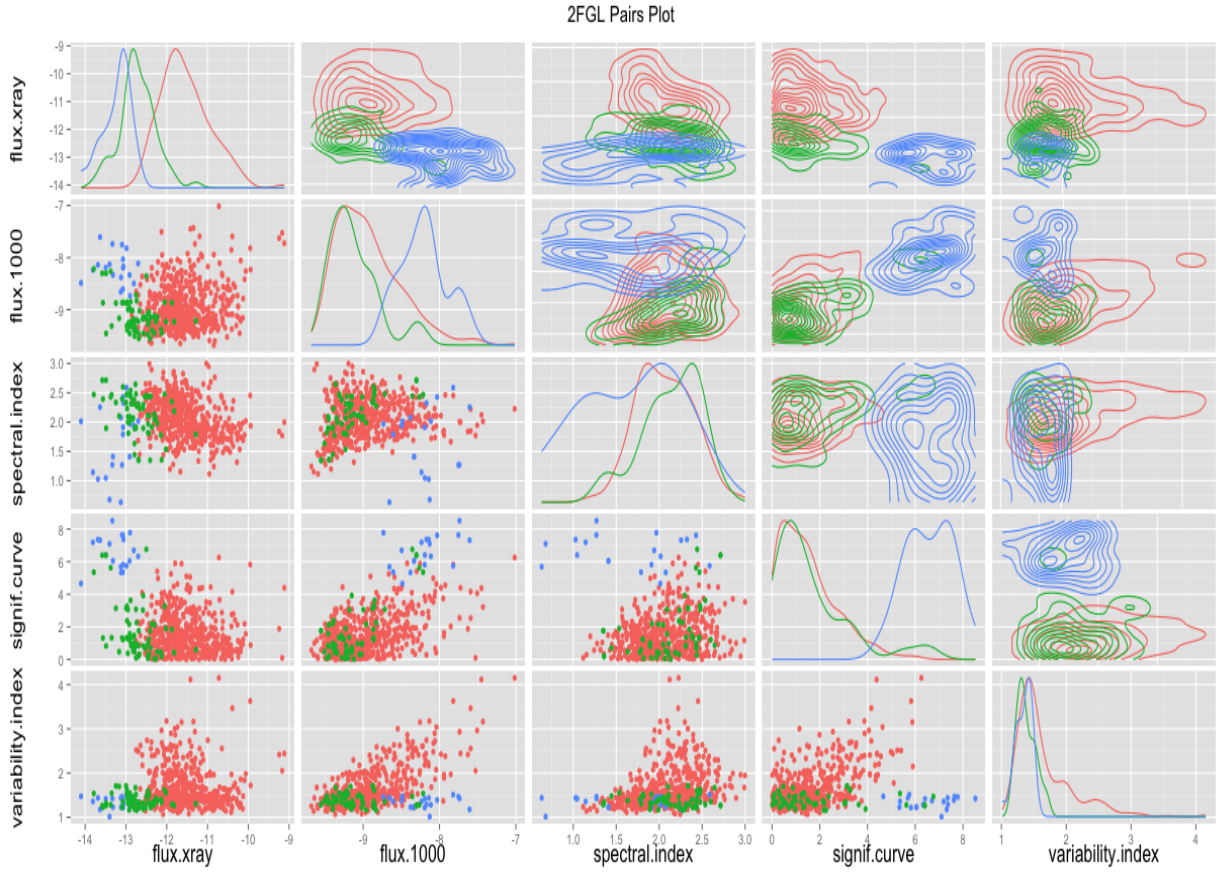


**Figure 9: Density plot of 2FGL data. Red points are known blazars, blue points are known pulsars, and green points are unassociated objects.**

# Chapter 6

## Results

After performing the knn tests on the two test sets of data we found that 104 1FGL notable excess were associated with blazars, 21 1FGL notable excesses were associated with pulsars, and all 66 2FGL notable excesses were associated with blazars. Of the 104 blazar associated 1FGL notable excesses, 75 were unique. Of the 21 pulsar associated 1FGL notable excesses, 8 were unique. Of the 66 blazar associated 2FGL notable excesses, 53 were unique. Therefore of the 136 unique 1FGL and 2FGL notable excesses that defined our test set of data, 128 were associated with blazars and 8 were associated with pulsars. These results, with association identification strengths obtained through the kknn analysis, are displayed in Table 3 and Table 4.

**Table 3: 1FGL kknn results. The blazar factor and pulsar factors are the "probabilities" of blazar or pulsar likelihood as determined by the kknn package. These are not real probabilities but instead present how close the nearest neighbors are to the test set point.**

| 1FGL Name | Swift Excess Name | KKNN Association | KKNN Blazar Factor | KKNN Pulsar Factor |
|---|---|---|---|---|
| J0001.9-4158 | J000132.8-415522 | blazar | 1.0000 | 0.0000 |
| J0003.1+6227 | J000340.2+622526 | blazar | 0.5772 | 0.4228 |
| J0009.1+5031 | J000922.4+503031 | blazar | 1.0000 | 0.0000 |
| J0131.2+6121 | J013106.8+612035 | blazar | 1.0000 | 0.0000 |
| J0137.8+5814 | J013750.3+581411 | blazar | 1.0000 | 0.0000 |
| J0143.9-5845 | J014347.4-584552 | blazar | 1.0000 | 0.0000 |
| J0212.3+5319 | J021210.5+532136 | blazar | 1.0000 | 0.0000 |
| J0223.0-1118 | J022314.3-111739 | blazar | 1.0000 | 0.0000 |
| J0316.3-6438 | J031614.1-643730 | blazar | 1.0000 | 0.0000 |
| J0335.5-4501 | J033513.7-445943 | blazar | 1.0000 | 0.0000 |
| J0409.9-0357 | J040946.6-040000 | blazar | 1.0000 | 0.0000 |
| J0430.3+3511c | J043041.1+351353 | blazar | 1.0000 | 0.0000 |
| J0430.3+3511c | J043000.9+351723 | blazar | 1.0000 | 0.0000 |
| J0430.3+3511c | J043019.3+351744 | blazar | 1.0000 | 0.0000 |

| 1FGL Name | Swift Excess Name | KKNN Association | KKNN Blazar Factor | KKNN Pulsar Factor |
|---|---|---|---|---|
| J0430.3+3511c | J043013.7+351339 | blazar | 1.0000 | 0.0000 |
| J0430.3+3511c | J043103.5+350915 | blazar | 1.0000 | 0.0000 |
| J0521.6+0103 | J052141.2+010251 | blazar | 1.0000 | 0.0000 |
| J0521.6+0103 | J052153.10+005936 | blazar | 1.0000 | 0.0000 |
| J0521.6+0103 | J052203.0+010552 | blazar | 1.0000 | 0.0000 |
| J0523.5-2529 | J052316.5-252737 | blazar | 0.7502 | 0.2498 |
| J0523.5-2529 | J052323.9-252731 | blazar | 0.7502 | 0.2498 |
| J0534.7-0531c | J053456.5-053136 | blazar | 0.9363 | 0.0637 |
| J0534.7-0531c | J053427.7-053154 | blazar | 0.9363 | 0.0637 |
| J0534.7-0531c | J053434.0-052821 | blazar | 0.9363 | 0.0637 |
| J0534.7-0531c | J053503.5-052952 | blazar | 0.9363 | 0.0637 |
| J0534.7-0531c | J053440.1-052642 | blazar | 0.9363 | 0.0637 |
| J0534.7-0531c | J053455.8-052916 | blazar | 0.9363 | 0.0637 |
| J0534.7-0531c | J053435.2-053210 | blazar | 0.9363 | 0.0637 |
| J0536.2-0607c | J053631.4-060826 | blazar | 1.0000 | 0.0000 |
| J0536.2-0607c | J053622.3-060228 | blazar | 1.0000 | 0.0000 |
| J0605.3+3800 | J060503.5+375738 | blazar | 1.0000 | 0.0000 |
| J0648.8+1516 | J064847.6+151623 | blazar | 1.0000 | 0.0000 |
| J0659.9+1303 | J070014.3+130423 | blazar | 1.0000 | 0.0000 |
| J0734.7-1557 | J073437.6-155612 | blazar | 0.6367 | 0.3633 |
| J0744.1-2523 | J074346.6-252510 | blazar | 0.9363 | 0.0637 |
| J0746.5-0711 | J074639.8-071716 | blazar | 1.0000 | 0.0000 |
| J0823.3-4248 | J082324.7-425012 | pulsar | 0.0201 | 0.9799 |
| J0823.3-4248 | J082334.3-424631 | pulsar | 0.0201 | 0.9799 |
| J0823.3-4248 | J082336.1-424717 | pulsar | 0.0201 | 0.9799 |
| J0823.3-4248 | J082328.10-425136 | pulsar | 0.0201 | 0.9799 |
| J0823.3-4248 | J082341.1-425050 | pulsar | 0.0201 | 0.9799 |
| J0823.3-4248 | J082328.1-424354 | pulsar | 0.0201 | 0.9799 |
| J0823.3-4248 | J082304.7-425214 | pulsar | 0.0201 | 0.9799 |
| J0823.3-4248 | J082310.1-425001 | pulsar | 0.0201 | 0.9799 |
| J0823.3-4248 | J082317.9-424933 | pulsar | 0.0201 | 0.9799 |
| J0838.6-2828 | J083843.4-282701 | blazar | 1.0000 | 0.0000 |
| J0841.4-3558 | J084121.7-355507 | blazar | 1.0000 | 0.0000 |
| J0841.4-3558 | J084121.3-355715 | blazar | 1.0000 | 0.0000 |
| J0848.6+0504 | J084839.6+050620 | blazar | 1.0000 | 0.0000 |
| J0849.4-2912 | J084900.10-291149 | blazar | 1.0000 | 0.0000 |

| 1FGL Name | Swift Excess Name | KKNN Association | KKNN Blazar Factor | KKNN Pulsar Factor |
|---|---|---|---|---|
| J0908.7-2119 | J090858.6-211852 | blazar | 1.0000 | 0.0000 |
| J0922.0+2337 | J092145.2+233547 | blazar | 1.0000 | 0.0000 |
| J1033.5-5033 | J103332.4-503526 | blazar | 1.0000 | 0.0000 |
| J1040.5+0616 | J104031.7+061722 | blazar | 1.0000 | 0.0000 |
| J1040.5+0616 | J104039.4+061523 | blazar | 1.0000 | 0.0000 |
| J1040.5+0616 | J104048.4+061821 | blazar | 1.0000 | 0.0000 |
| J1040.9-1205 | J104108.6-120330 | blazar | 1.0000 | 0.0000 |
| J1040.9-1205 | J104048.6-120618 | blazar | 1.0000 | 0.0000 |
| J1110.3-1622 | J111017.10-162401 | blazar | 1.0000 | 0.0000 |
| J1115.2-6124c | J111453.3-612421 | blazar | 1.0000 | 0.0000 |
| J1117.0-5339 | J111715.2-533816 | blazar | 1.0000 | 0.0000 |
| J1119.9-2205 | J111959.1-220455 | pulsar | 0.4228 | 0.5772 |
| J1119.9-2205 | J111952.7-220637 | pulsar | 0.4228 | 0.5772 |
| J1119.9-2205 | J112010.2-220811 | pulsar | 0.4228 | 0.5772 |
| J1119.9-2205 | J112001.1-220130 | pulsar | 0.4228 | 0.5772 |
| J1123.6-4555 | J112355.5-455019 | blazar | 1.0000 | 0.0000 |
| J1141.8-1403 | J114141.7-140755 | blazar | 1.0000 | 0.0000 |
| J1221.4-0635 | J122127.2-062847 | blazar | 1.0000 | 0.0000 |
| J1223.4-3034 | J122336.9-303250 | blazar | 1.0000 | 0.0000 |
| J1226.0+2954 | J122608.3+295942 | blazar | 1.0000 | 0.0000 |
| J1227.9-4852 | J122758.7-485342 | blazar | 1.0000 | 0.0000 |
| J1227.9-4852 | J122724.8-485555 | blazar | 1.0000 | 0.0000 |
| J1227.9-4852 | J122742.9-485225 | blazar | 1.0000 | 0.0000 |
| J1227.9-4852 | J122823.1-485038 | blazar | 1.0000 | 0.0000 |
| J1240.3-7154 | J124021.4-714858 | blazar | 1.0000 | 0.0000 |
| J1249.3-2812 | J124919.4-280832 | blazar | 1.0000 | 0.0000 |
| J1250.9-4940 | J125058.8-494447 | blazar | 1.0000 | 0.0000 |
| J1256.1-5922 | J125605.9-591941 | blazar | 1.0000 | 0.0000 |
| J1258.3+2125 | J125821.5+212351 | blazar | 1.0000 | 0.0000 |
| J1306.4-6038 | J130601.9-603358 | pulsar | 0.4430 | 0.5570 |
| J1322.1+0838 | J132210.2+084231 | blazar | 1.0000 | 0.0000 |
| J1322.1+0838 | J132222.9+084320 | blazar | 1.0000 | 0.0000 |
| J1340.5-0413 | J134042.1-041008 | blazar | 1.0000 | 0.0000 |
| J1353.6-6640 | J135339.10-664000 | blazar | 1.0000 | 0.0000 |
| J1412.6+7406 | J141234.9+741158 | blazar | 1.0000 | 0.0000 |
| J1419.7+7731 | J141901.2+773228 | blazar | 1.0000 | 0.0000 |

| 1FGL Name | Swift Excess Name | KKNN Association | KKNN Blazar Factor | KKNN Pulsar Factor |
|---|---|---|---|---|
| J1446.8-4702 | J144719.8-470102 | blazar | 1.0000 | 0.0000 |
| J1511.8-0513 | J151148.6-051347 | blazar | 1.0000 | 0.0000 |
| J1511.8-0513 | J151200.1-051528 | blazar | 1.0000 | 0.0000 |
| J1511.9-2253 | J151212.8-225506 | blazar | 1.0000 | 0.0000 |
| J1511.9-2253 | J151137.1-225744 | blazar | 1.0000 | 0.0000 |
| J1539.0-3328 | J153924.7-332839 | pulsar | 0.1772 | 0.8228 |
| J1539.0-3328 | J153900.6-332702 | pulsar | 0.1772 | 0.8228 |
| J1549.7-0659 | J154952.1-065908 | blazar | 1.0000 | 0.0000 |
| J1625.8-2429c | J162558.1-243029 | pulsar | 0.3336 | 0.6664 |
| J1639.5-5152 | J163926.3-514933 | blazar | 1.0000 | 0.0000 |
| J1650.3-5410 | J165043.10-540508 | blazar | 1.0000 | 0.0000 |
| J1656.2-3257 | J165616.9-330211 | blazar | 1.0000 | 0.0000 |
| J1656.2-3257 | J165557.8-325946 | blazar | 1.0000 | 0.0000 |
| J1816.7+4509 | J181652.5+450731 | blazar | 1.0000 | 0.0000 |
| J1823.5-3454 | J182338.8-345412 | blazar | 1.0000 | 0.0000 |
| J1831.5-0200c | J183126.7-020518 | blazar | 0.5529 | 0.4471 |
| J1831.5-0200c | J183113.5-020350 | blazar | 0.5529 | 0.4471 |
| J1835.3+1345 | J183539.5+135048 | blazar | 1.0000 | 0.0000 |
| J1842.3-5845 | J184229.10-584158 | blazar | 1.0000 | 0.0000 |
| J1844.1+1547 | J184425.4+154643 | blazar | 1.0000 | 0.0000 |
| J1857.1+0212c | J185651.5+021023 | pulsar | 0.2367 | 0.7633 |
| J1933.3+0723 | J193320.2+072619 | blazar | 1.0000 | 0.0000 |
| J1942.7+1033 | J194247.5+103327 | blazar | 1.0000 | 0.0000 |
| J2004.8+7004 | J200505.5+700437 | blazar | 1.0000 | 0.0000 |
| J2014.4+0647 | J201431.1+064850 | blazar | 1.0000 | 0.0000 |
| J2014.4+0647 | J201410.9+064354 | blazar | 1.0000 | 0.0000 |
| J2034.6-4202 | J203450.8-420038 | blazar | 1.0000 | 0.0000 |
| J2037.0-3329 | J203649.6-332829 | blazar | 1.0000 | 0.0000 |
| J2043.2+1709 | J204312.9+171019 | pulsar | 0.2568 | 0.7432 |
| J2043.2+1709 | J204318.7+170755 | pulsar | 0.2568 | 0.7432 |
| J2056.7+4938 | J205642.7+494008 | blazar | 1.0000 | 0.0000 |
| J2058.8-3903 | J205902.5-385936 | blazar | 1.0000 | 0.0000 |
| J2104.6+2119 | J210415.9+211807 | blazar | 1.0000 | 0.0000 |
| J2107.5+5202c | J210720.4+520257 | pulsar | 0.1973 | 0.8027 |
| J2129.8-0427 | J213008.1-043452 | blazar | 1.0000 | 0.0000 |
| J2129.8-0427 | J212945.4-042910 | blazar | 1.0000 | 0.0000 |

| 1FGL Name | Swift Excess Name | KKNN Association | KKNN Blazar Factor | KKNN Pulsar Factor |
|---|---|---|---|---|
| J2216.1+5139 | J221545.9+514454 | blazar | 0.7502 | 0.2498 |
| J2257.9-3643 | J225756.10-364607 | blazar | 1.0000 | 0.0000 |
| J2257.9-3643 | J225814.8-364430 | blazar | 1.0000 | 0.0000 |

**Table 4: 2FGL kknn results. The blazar factor and pulsar factors are the "probabilities" of blazar or pulsar likelihood as determined by the kknn package. These are not real probabilities but instead present how close the nearest neighbors are to the test set point.**

| 2FGL Name | Swift Excess Name | KKNN Association | KKNN Blazar Factor | KKNN Pulsar Factor |
|---|---|---|---|---|
| J0031.0+0724 | J003119.7+072451 | blazar | 1.0000 | 0.0000 |
| J0031.0+0724 | J003054.7+072325 | blazar | 1.0000 | 0.0000 |
| J0048.8-6347 | J004935.8-634745 | blazar | 1.0000 | 0.0000 |
| J0116.6-6153 | J011619.2-615341 | blazar | 1.0000 | 0.0000 |
| J0133.4-4408 | J013321.6-441314 | blazar | 1.0000 | 0.0000 |
| J0200.4-4105 | J020020.8-410933 | blazar | 1.0000 | 0.0000 |
| J0222.7+6820 | J022302.8+682157 | blazar | 1.0000 | 0.0000 |
| J0226.1+0943 | J022613.6+093723 | blazar | 1.0000 | 0.0000 |
| J0338.2+1306 | J033829.3+130215 | blazar | 1.0000 | 0.0000 |
| J0353.2+5653 | J035309.5+565428 | blazar | 1.0000 | 0.0000 |
| J0438.0-7331 | J043836.9-732920 | blazar | 1.0000 | 0.0000 |
| J0458.4+0654 | J045802.6+065012 | blazar | 1.0000 | 0.0000 |
| J0529.3+3821 | J052939.4+382323 | blazar | 1.0000 | 0.0000 |
| J0644.6+6034 | J064436.1+603852 | blazar | 1.0000 | 0.0000 |
| J0658.4+0633 | J065845.2+063711 | blazar | 1.0000 | 0.0000 |
| J0725.8-0549 | J072547.5-054830 | blazar | 1.0000 | 0.0000 |
| J0737.1-3235 | J073713.10-323627 | blazar | 1.0000 | 0.0000 |
| J0737.1-3235 | J073738.9-323257 | blazar | 1.0000 | 0.0000 |
| J0737.5-8246 | J073705.0-824842 | blazar | 1.0000 | 0.0000 |
| J0737.5-8246 | J073820.2-825042 | blazar | 1.0000 | 0.0000 |
| J0745.5+7910 | J074513.0+791315 | blazar | 1.0000 | 0.0000 |
| J0802.6-0940 | J080215.9-094214 | blazar | 1.0000 | 0.0000 |
| J0846.7-4053 | J084722.5-404736 | blazar | 1.0000 | 0.0000 |
| J0846.7-4053 | J084636.5-410300 | blazar | 1.0000 | 0.0000 |
| J0859.4-2532 | J085929.8-253107 | blazar | 1.0000 | 0.0000 |
| J0900.9+6736 | J090121.6+673956 | blazar | 1.0000 | 0.0000 |
| J0900.9+6736 | J090110.4+674203 | blazar | 1.0000 | 0.0000 |
| J0900.9+6736 | J090015.5+673809 | blazar | 1.0000 | 0.0000 |
| J0937.9-1434 | J093754.6-143349 | blazar | 1.0000 | 0.0000 |

| 2FGL Name | Swift Excess Name | KKNN Association | KKNN Blazar Factor | KKNN Pulsar Factor |
|---|---|---|---|---|
| J0937.9-1434 | J093738.2-142930 | blazar | 1.0000 | 0.0000 |
| J1013.6+3434 | J101351.5+343418 | blazar | 1.0000 | 0.0000 |
| J1016.4-4244 | J101620.7-424722 | blazar | 1.0000 | 0.0000 |
| J1016.4-4244 | J101635.5-424322 | blazar | 1.0000 | 0.0000 |
| J1029.5-2022 | J102946.8-201813 | blazar | 1.0000 | 0.0000 |
| J1038.2-2423 | J103755.0-242545 | blazar | 1.0000 | 0.0000 |
| J1038.2-2423 | J103748.3-242847 | blazar | 1.0000 | 0.0000 |
| J1056.2-6021 | J105645.1-601939 | blazar | 1.0000 | 0.0000 |
| J1058.7-6621 | J105832.1-662603 | blazar | 1.0000 | 0.0000 |
| J1105.4-7622 | J110451.2-762542 | blazar | 1.0000 | 0.0000 |
| J1105.4-7622 | J110409.3-762723 | blazar | 1.0000 | 0.0000 |
| J1105.4-7622 | J110552.1-761830 | blazar | 1.0000 | 0.0000 |
| J1105.6-6114 | J110506.4-611602 | blazar | 0.6367 | 0.3633 |
| J1105.6-6114 | J110619.3-611419 | blazar | 0.6367 | 0.3633 |
| J1259.8-3749 | J125949.7-374856 | blazar | 1.0000 | 0.0000 |
| J1317.2-6304 | J131710.7-630211 | blazar | 1.0000 | 0.0000 |
| J1347.0-2956 | J134706.8-295842 | blazar | 1.0000 | 0.0000 |
| J1347.0-2956 | J134702.8-295216 | blazar | 1.0000 | 0.0000 |
| J1424.2-1752 | J142412.5-175008 | blazar | 1.0000 | 0.0000 |
| J1502.1+5548 | J150217.7+554512 | blazar | 1.0000 | 0.0000 |
| J1617.3-5336 | J161646.7-534340 | blazar | 1.0000 | 0.0000 |
| J1659.2-0142 | J165922.2-014110 | blazar | 1.0000 | 0.0000 |
| J1704.3+1235 | J170409.6+123423 | blazar | 1.0000 | 0.0000 |
| J1704.6-0529 | J170433.9-052840 | blazar | 1.0000 | 0.0000 |
| J1726.6-3545 | J172641.8-354053 | blazar | 0.5066 | 0.4934 |
| J1813.6-2821 | J181357.8-282043 | blazar | 1.0000 | 0.0000 |
| J1828.7+3231 | J182915.5+323432 | blazar | 1.0000 | 0.0000 |
| J1842.3-5839 | J184230.0-584158 | blazar | 1.0000 | 0.0000 |
| J1904.8-0705 | J190444.5-070743 | blazar | 1.0000 | 0.0000 |
| J1908.8-0132 | J190843.4-012954 | blazar | 1.0000 | 0.0000 |
| J1924.9-1036 | J192501.5-104317 | blazar | 1.0000 | 0.0000 |
| J2115.4+1213 | J211522.1+121801 | blazar | 1.0000 | 0.0000 |
| J2133.5-6431 | J213311.2-643819 | blazar | 1.0000 | 0.0000 |
| J2237.2+6316 | J223704.3+632336 | blazar | 1.0000 | 0.0000 |
| J2237.2+6316 | J223646.1+631605 | blazar | 1.0000 | 0.0000 |
| J2249.1+5758 | J224907.5+580304 | blazar | 1.0000 | 0.0000 |
| J2351.6-7558 | J235115.10-760016 | blazar | 1.0000 | 0.0000 |

Once the associations for the notable excesses were determined as outlined by Table 3 and Table 4, we created new plots reminiscent of the pair plots in Figure 8 and Figure 9 to obtain confidence in our determined results. These pair plots differed from Figure 8 and Figure 9 in that we plotted the test set points with their assigned association to view the distribution of associations. It should be noted that since all the 2FGL notable excesses were classified as blazars, a new pairs plot would have been redundant. The pairs plot of the associated 1FGL data is shown in Figure 10 below, with individual zoomed in plots displayed in Appendix B.

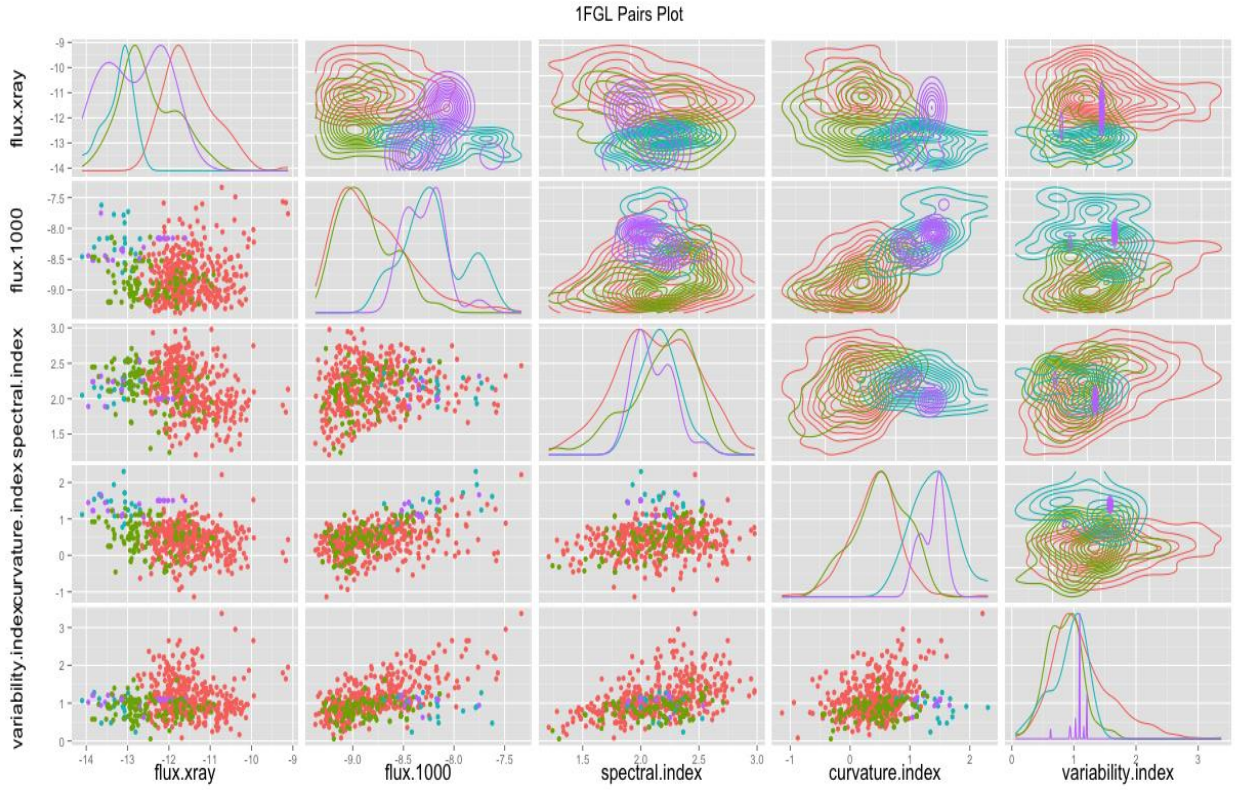


**Figure 10: 1FGL pairs plot. The red points are known blazars, the blue points are known pulsars, the green points are unassociated objects identified through kknn analysis as blazars, and the purple are unassociated objects identified as pulsars.**

The pairs plot and relevant plots included in Appendix B visually show that the kknn function performed a reliable association of the 1FGL notable excesses. Through visual analysis of the association for the 2FGL notable excesses we note that there appears to be some issues

with the kknn test, as objects that appear to clearly be associated with pulsars, are identified as blazars. These issues are discussed in more detail in the discussion but we note that these issues can be seen more significantly in the 2FGL plots displayed in Appendix A.

# Chapter 7

## Discussion

From the analysis that was performed for this thesis we have shown that by utilizing X-ray flux data we can significantly enhance the data mining and machine learning techniques that have been used on only *Fermi* data in the past (Ackermann et al., 2012; Mirabal et al., 2012; Hassan et al., 2013; Doert et al., 2014) to attempt to associate the still unassociated *Fermi* objects. From simply visually looking at the scatter plots created by plotting the X-ray flux versus observed *Fermi* variables such as gamma-ray flux, variability index, curvature index/curvature significance, and spectral index as shown in Appendix A, distinctions can be seen and crude associations can be made. This analysis certainly sets the stage for future attempts at associating objects in the 3FGL catalog and future catalogs and shows that multi-wavelength analysis rather than just gamma-ray analysis will result in the most precise associations.

From our knn test analysis we report 8 unique associations of pulsars and 128 unique associations of blazars from the 136 unique unassociated objects considered. While our knn test does provide nice simple results, the specific associations and reported probability factors obtained through the kknn function should be considered with some caution. There are issues associated with knn tests that can result in improper identifications and unrealistic probabilities. Performing multiple knn tests and visually interpreting the data can alleviate these issues to some extent. Through the use of the knn test in the "class" CRAN package (Venables & Ripley, 2002) we were able to confirm our associations through a separate knn analysis. Through visual analysis we obtained confidence in our results for the 1FGL identifications but discrepancies

arose when visually interpreting the 2FGL data. As has been stated previously, all 66 notable 2FGL excesses were identified as blazars. We expected the majority of associated objects to be identified as blazars but some pulsar identifications were also expected, especially for the 2FGL results due to the inclusion of galactic plane data points. Furthermore, in looking at the specific plots such as Figure 22 and Figure 30 in Appendix A it appears as if a handful of the test set points are associated with pulsars but our kknn analysis did not show this. We therefore report our results, with the caution that other analyses are required to trust these associations

The next step in this analysis would then be to attempt more significant data mining techniques, such as logistic regression, principle component analysis, or classification trees to obtain probabilities on potential associations. Once associations can be trusted to within certain significance, observers will be able to target specific unassociated objects in the *Fermi* catalogs with the idea of what they should be observing. This will allow for more efficient telescope time and our understanding of the different gamma-ray emitting objects in the universe will increase significantly. Data mining statistical analyses such as the one performed in this thesis will continue to be important for large astronomical datasets and push the field of astronomy forward as statistical approaches become better.

In addition to performing more statistical data mining analyses follow up observations of unassociated objects and multi-wavelength observations of known *Fermi* objects will significantly aid in the association and understanding of high-energy astrophysical phenomena. Through the comparison of variables at longer wavelengths than those examined in this thesis, such as radio and UV, further constraints can be placed on the training sets in parameter space, which will allow separations to become clear, and associations to be trusted more.

Our analysis shows that the identification and understanding of high-energy phenomena is becoming exponentially closer with each statistical and observational analysis and our picture of the universe is becoming much clearer. With the advancement in technology, computer power, and intellectual thinking, breakthroughs in the complete understanding in the physical processes of high-energy objects are on the horizon.

# Appendix A

## 1FGL and 2FGL Individual Plots Before Associations

This appendix lists the individual plots as seen in the pairs plot of Figure 8 and Figure 9 for the 1FGL and 2FGL notable excesses. Here we show the various variables for the unassociated test set data and the training sets plotted against each other in the search for clear separations. In these plots the red circles signify known blazars, the blue squares signify known pulsars, and the green triangles signify the appropriate unassociated test set objects.

### 1FGL Plots

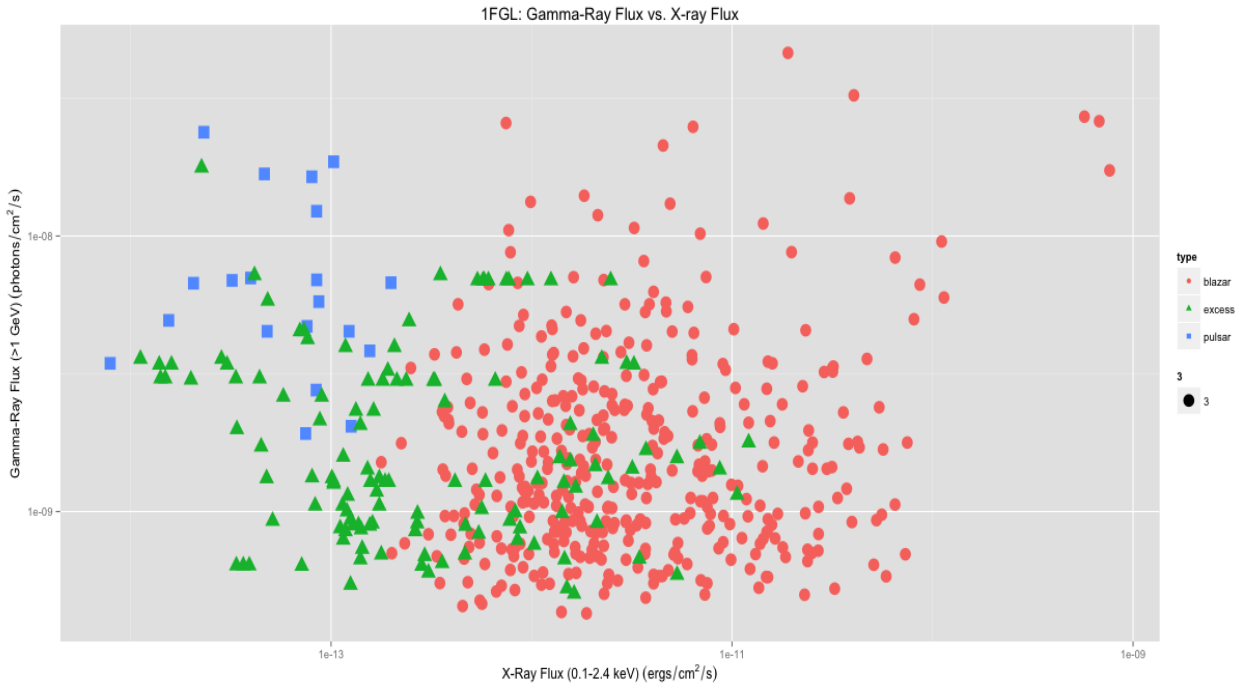


Figure 11: 1FGL - Gamma Ray Flux vs. X-ray Flux

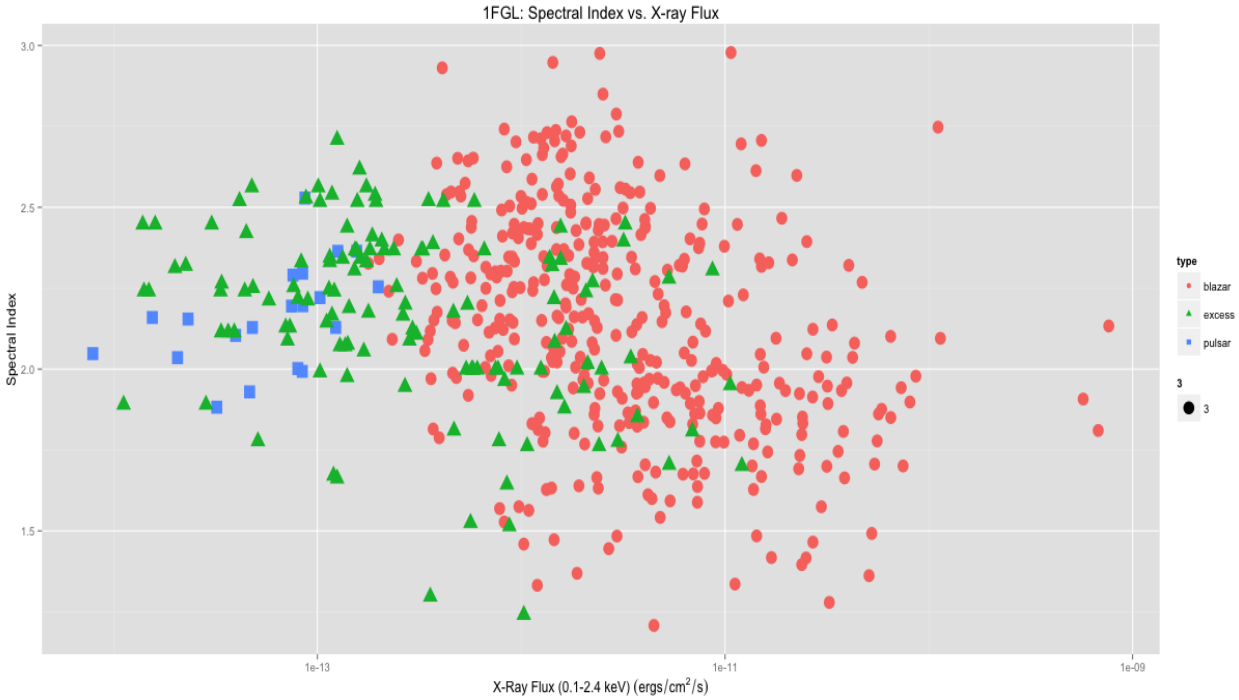


**Figure 12: 1FGL - Spectral Index vs. X-ray Flux**

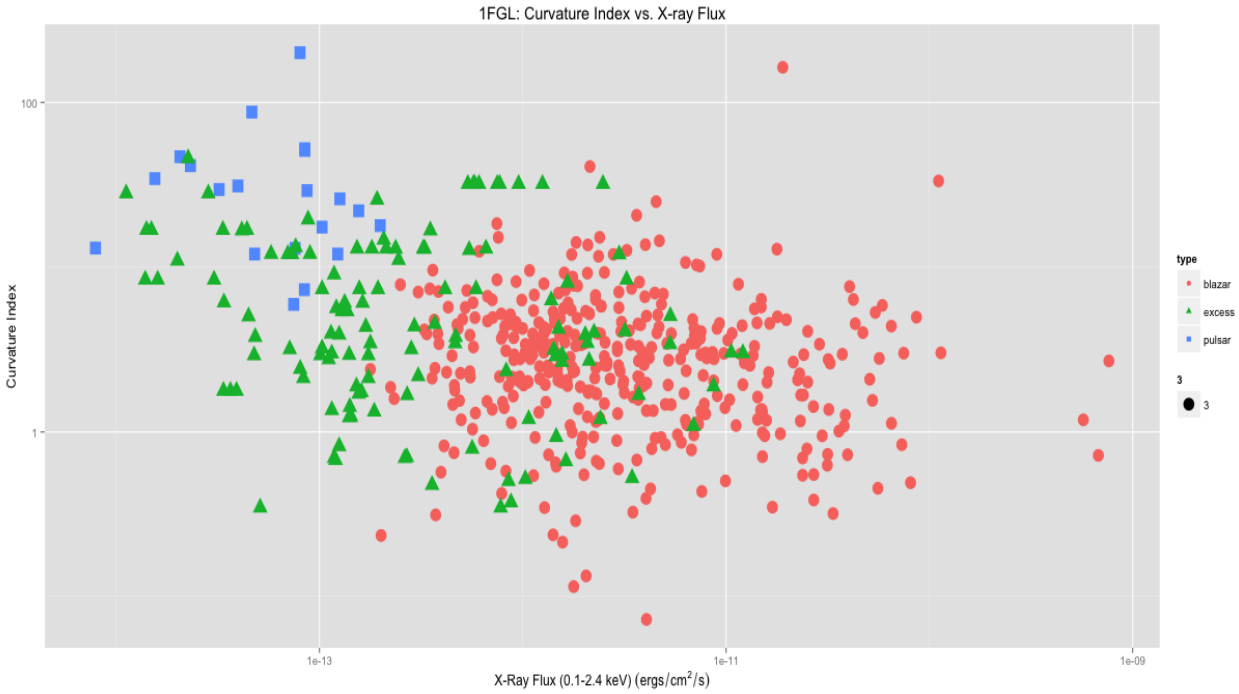


**Figure 13: 1FGL - Curvature Index vs. X-ray Flux**

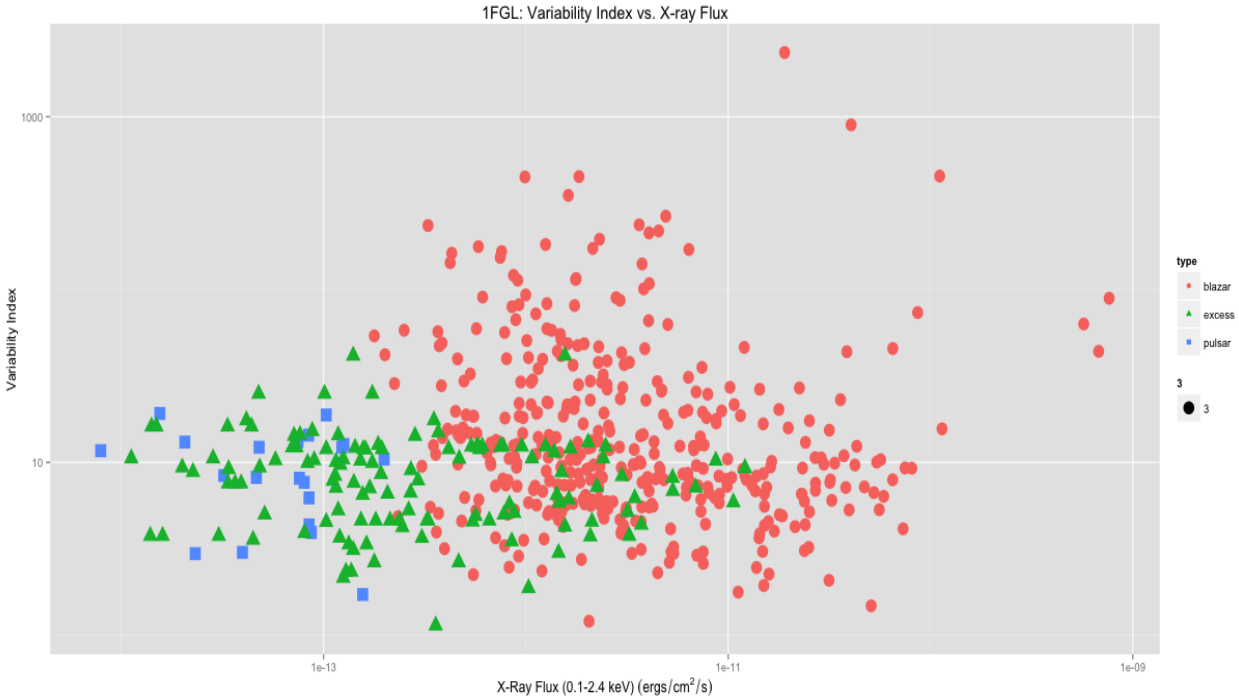


**Figure 14: 1FGL – Variability Index vs. X-ray Flux**

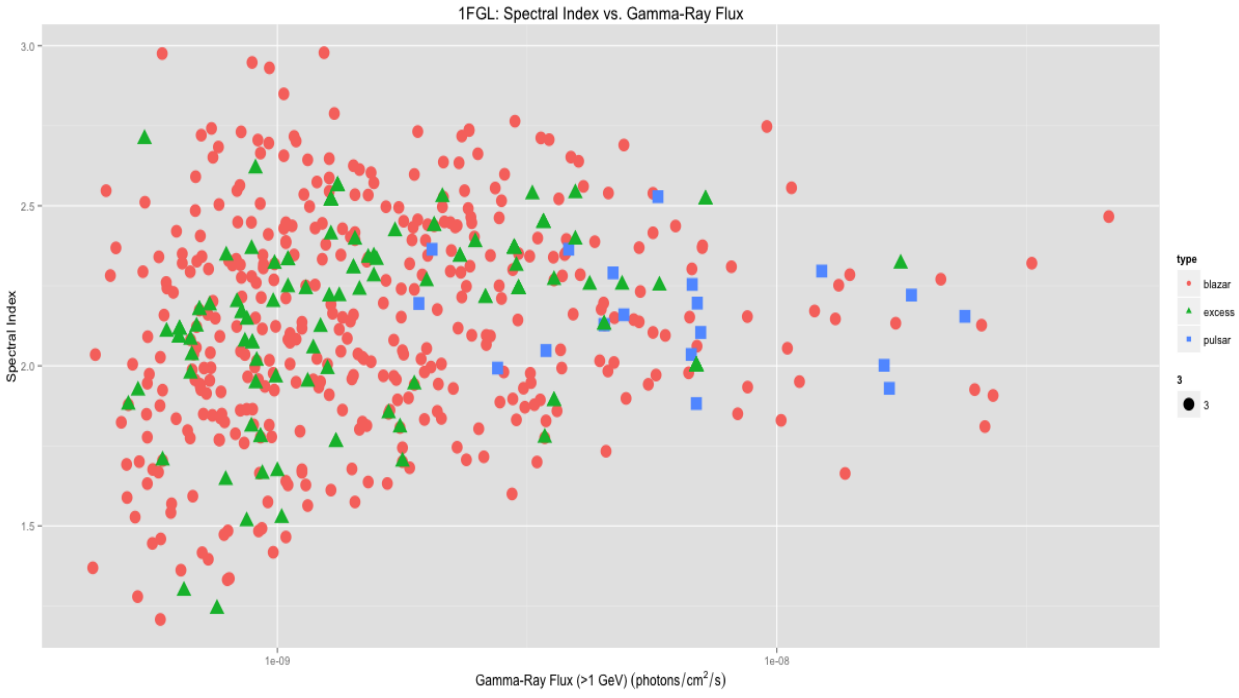


**Figure 15: 1FGL - Spectral Index vs. Gamma-Ray Flux**

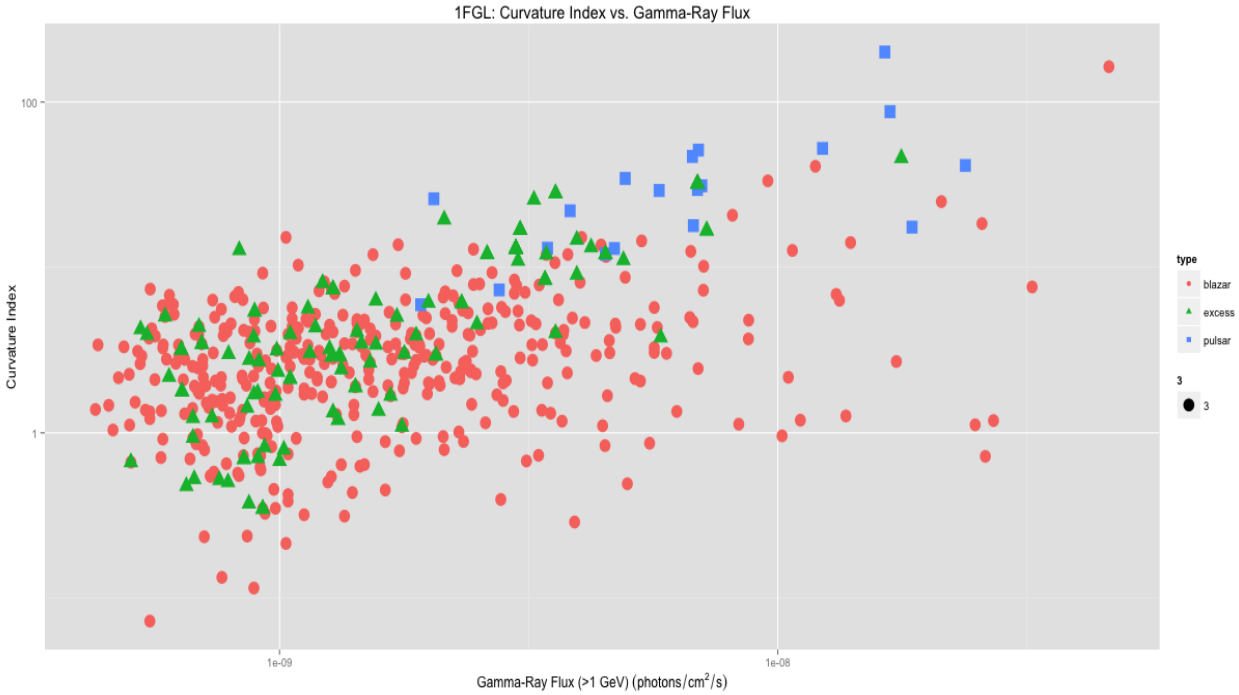


**Figure 16: 1FGL – Curvature Index vs. Gamma-Ray Flux**

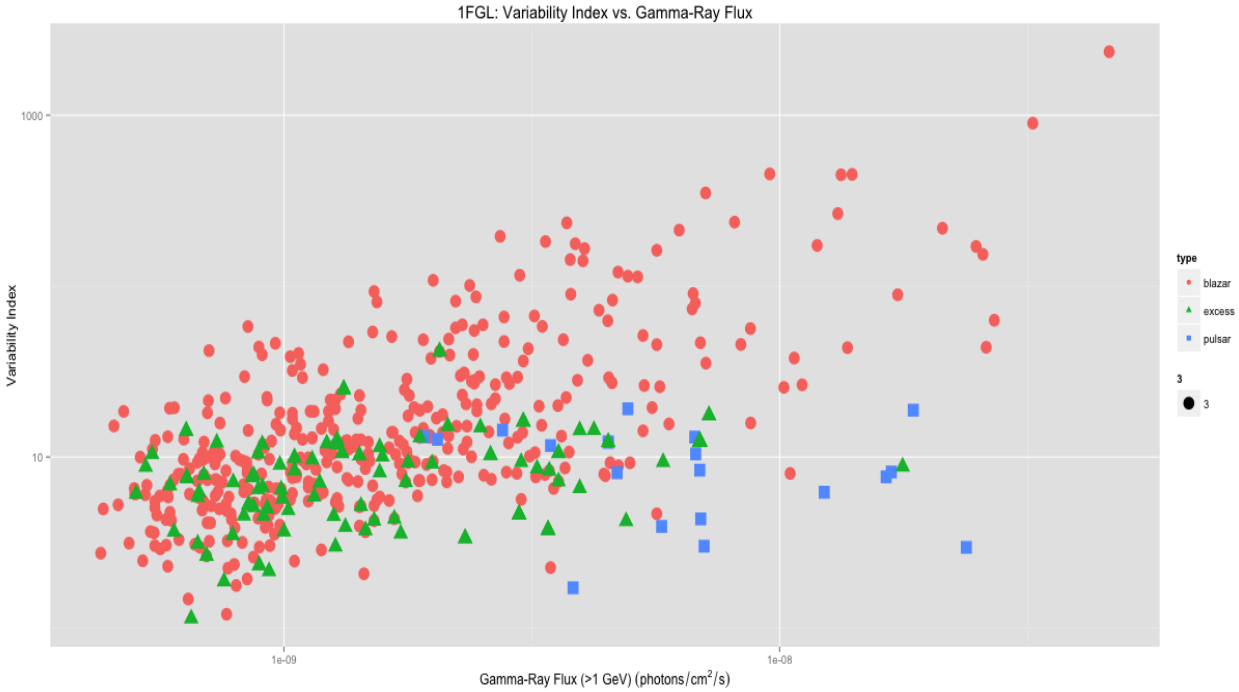


**Figure 17: 1FGL – Variability Index vs. Gamma-Ray Flux**

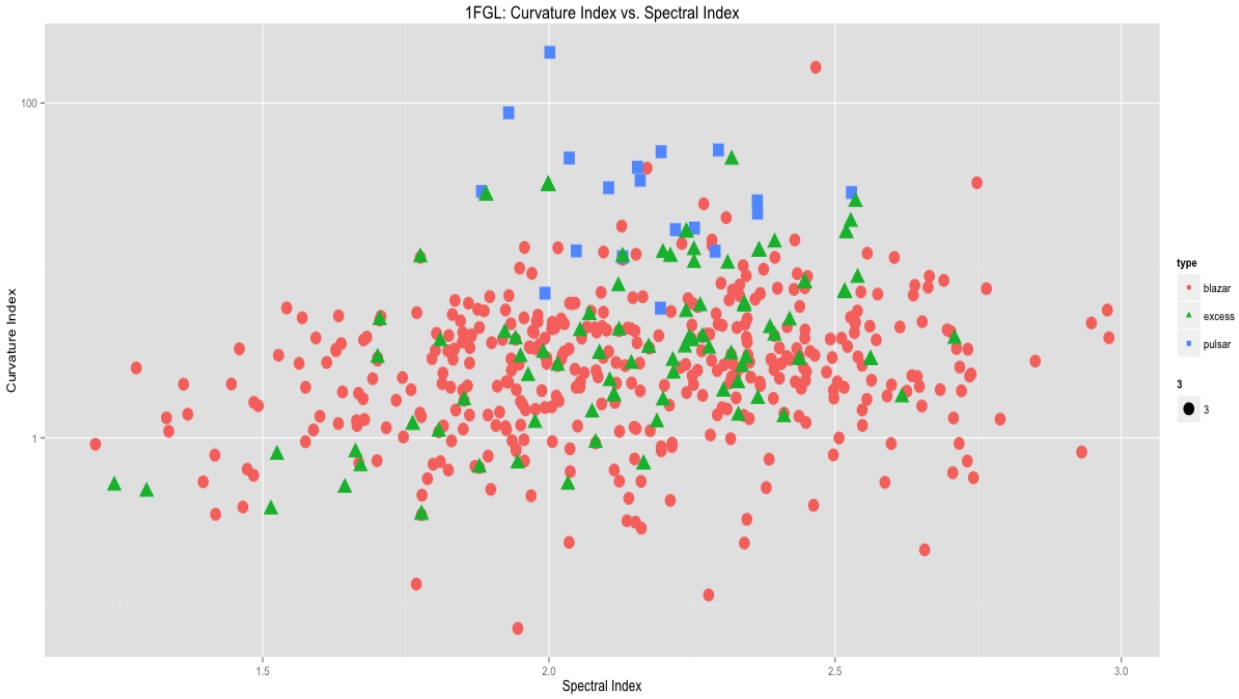


Figure 18: 1FGL – Curvature Index vs. Spectral Index

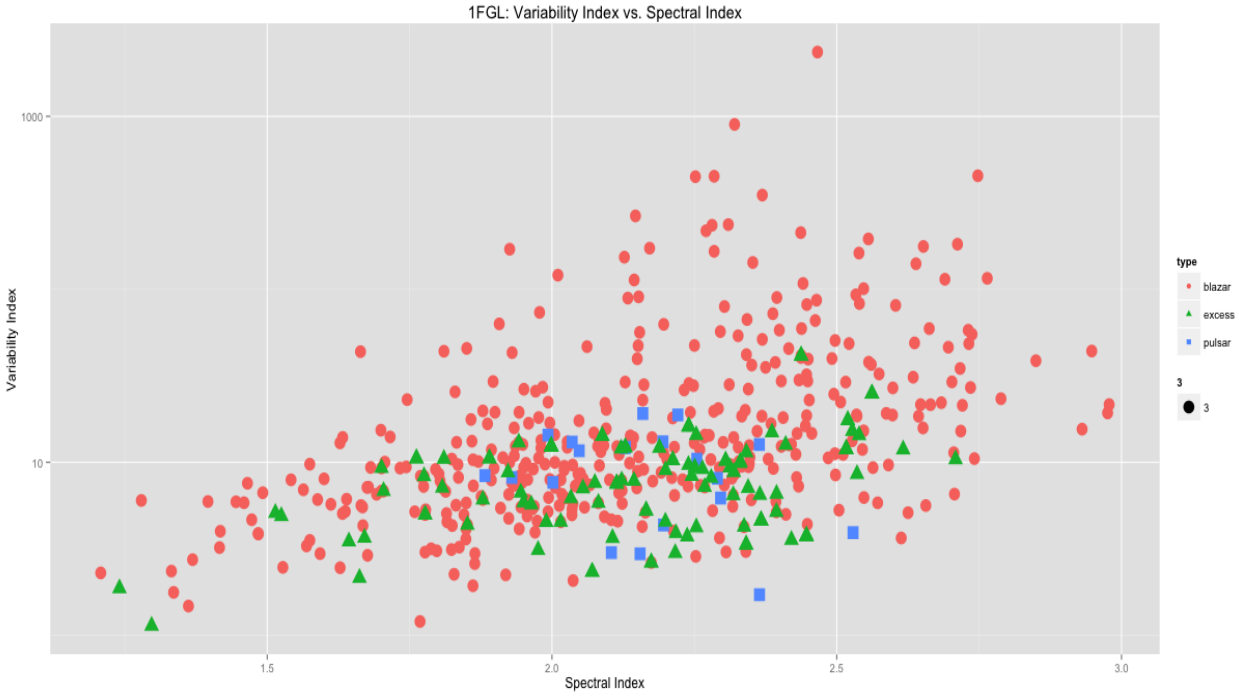


Figure 19: 1FGL – Variability Index vs. Spectral Index

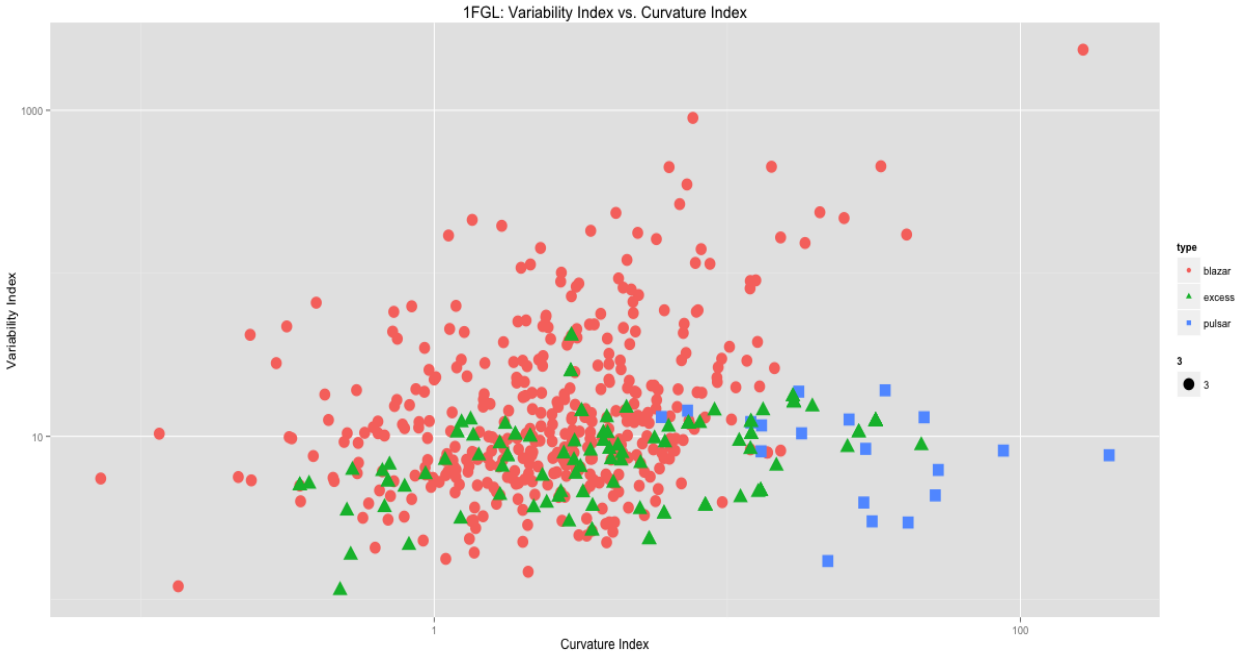


Figure 20: 1FGL – Variability Index vs. Curvature Index

## 2FGL Plots

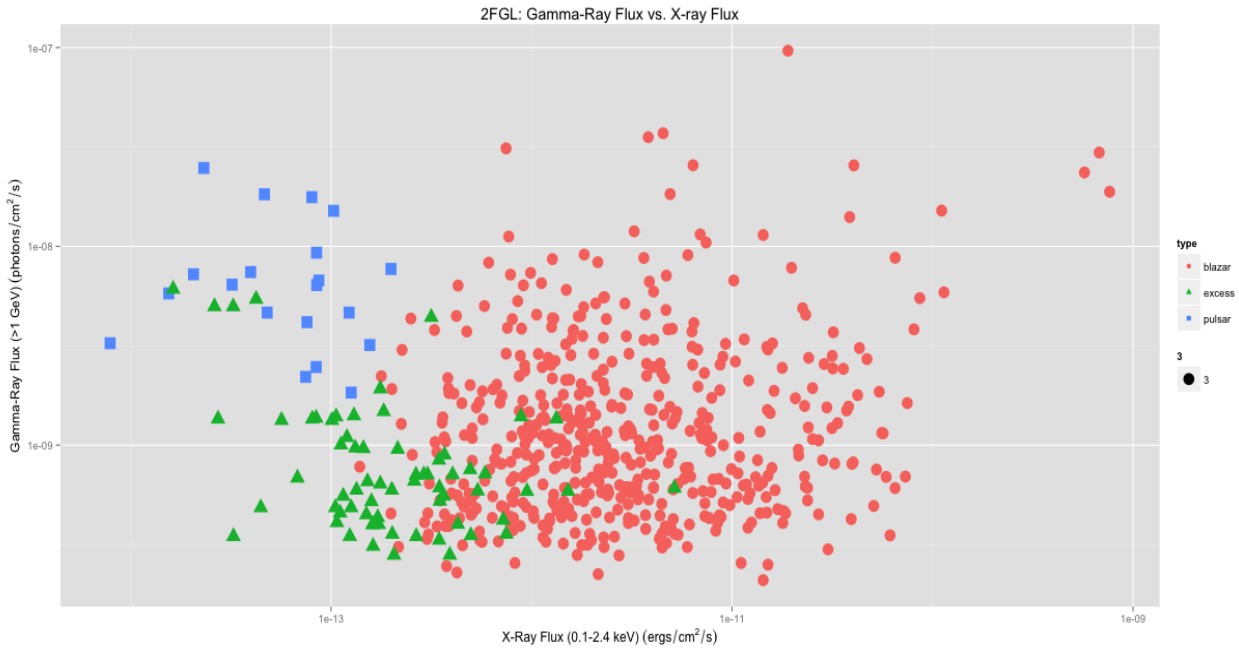


Figure 21: 2FGL – Gamma-Ray Flux vs. X-ray Flux

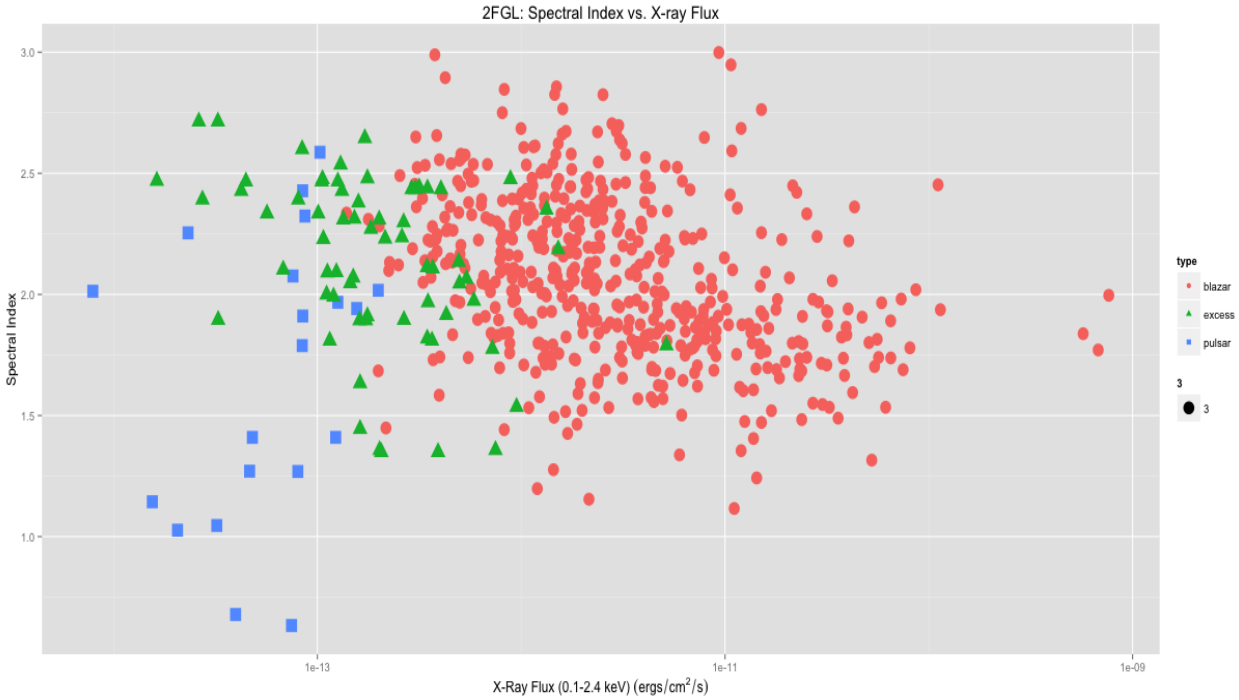


**Figure 22: 2FGL – Spectral Index vs. X-ray Flux**

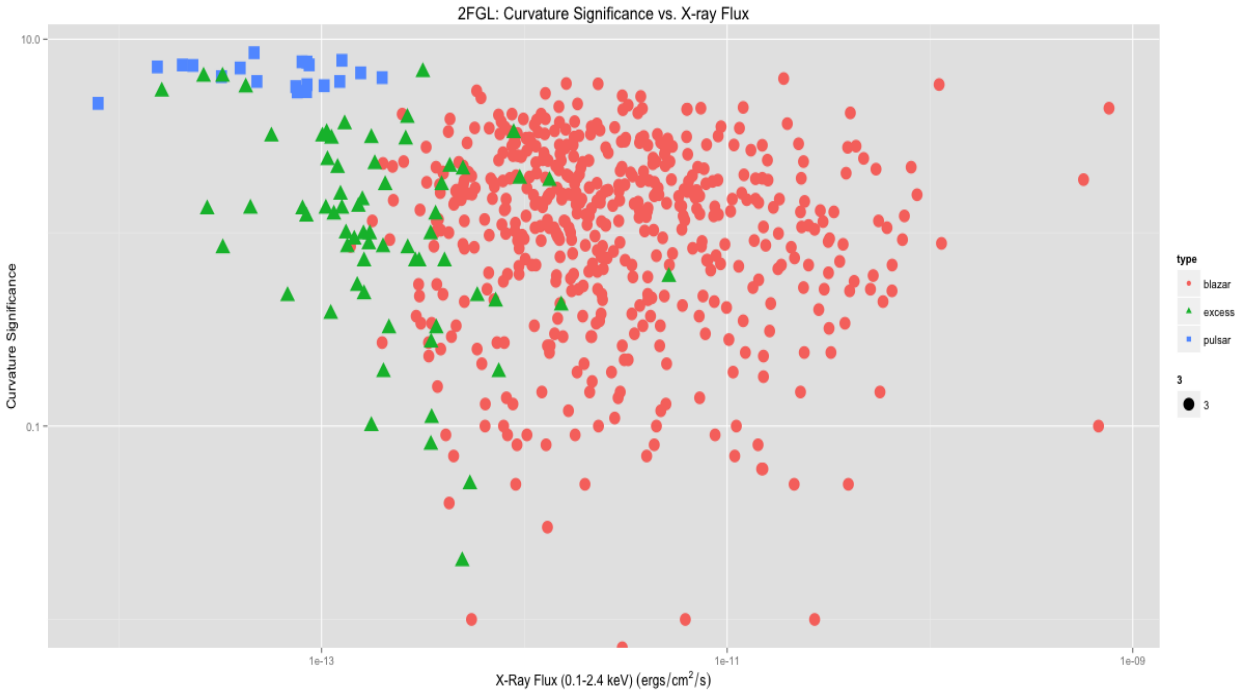


**Figure 23: 2FGL – Curvature Significance vs. X-ray Flux**

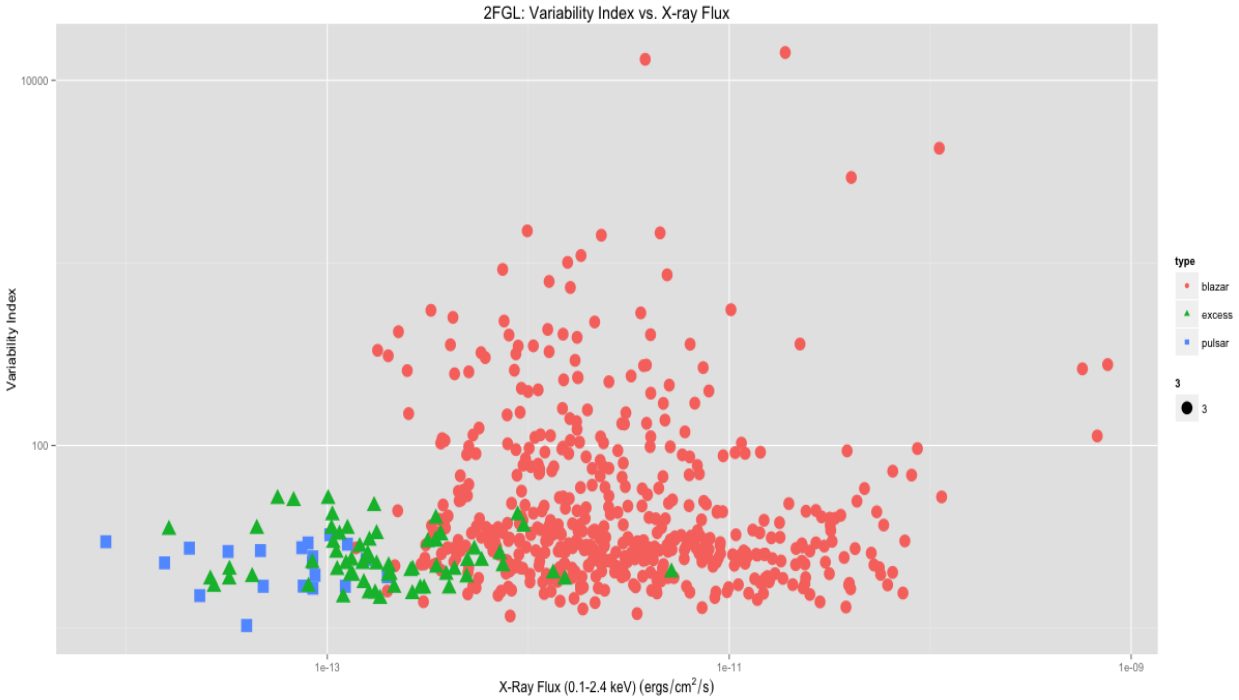


**Figure 24: 2FGL – Variability Index vs. X-ray Flux**

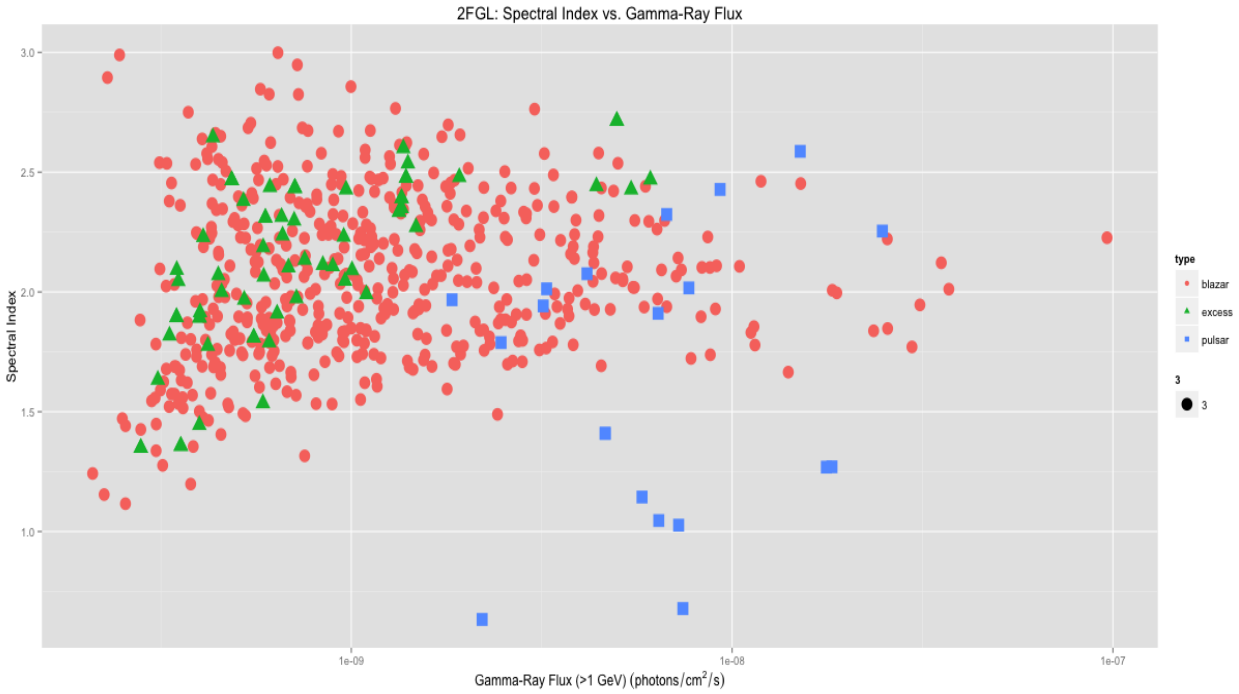


**Figure 25: 2FGL – Spectral Index vs. Gamma-Ray Flux**

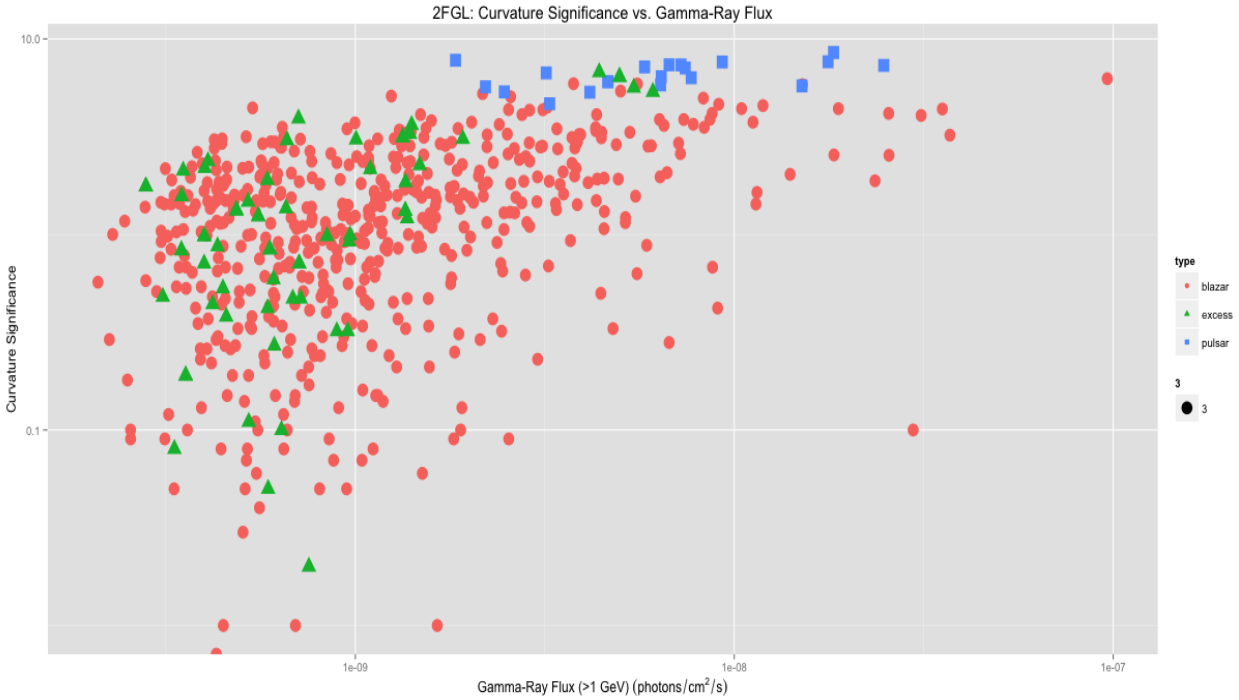


**Figure 26: 2FGL – Curvature Significance vs. Gamma-Ray Flux**

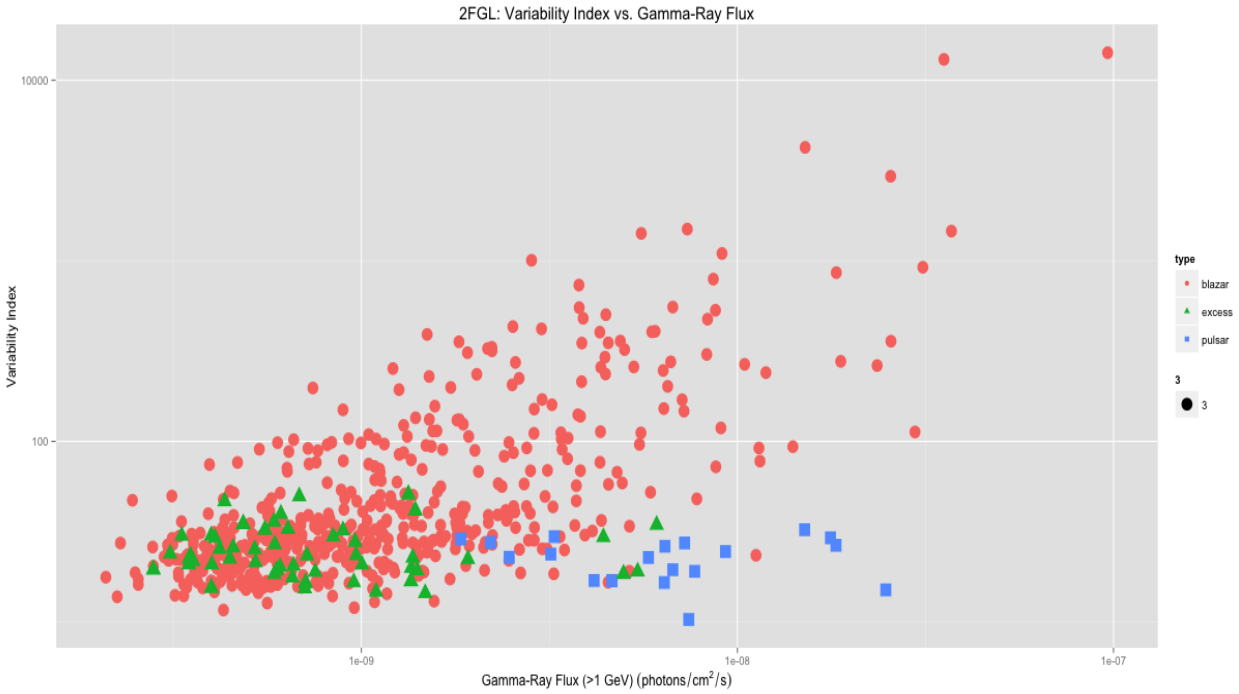


**Figure 27: 2FGL – Variability Index vs. Gamma-Ray Flux**

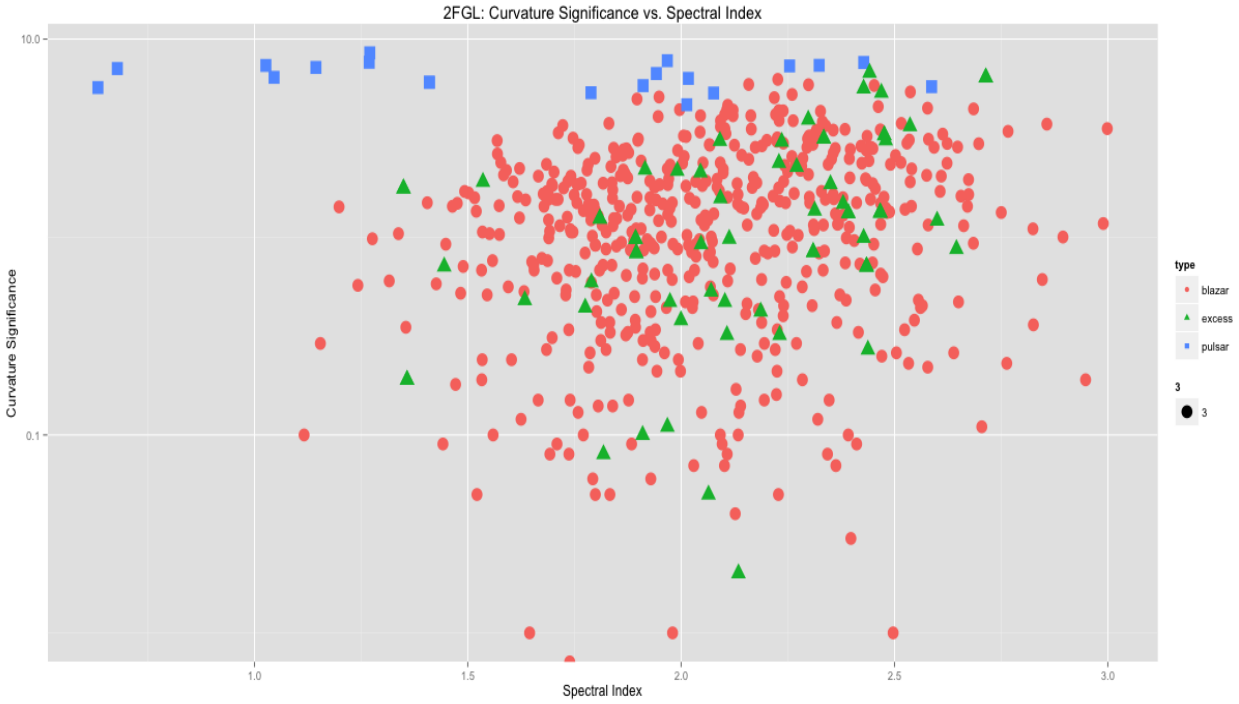


Figure 28: 2FGL – Curvature Significance vs. Spectral Index

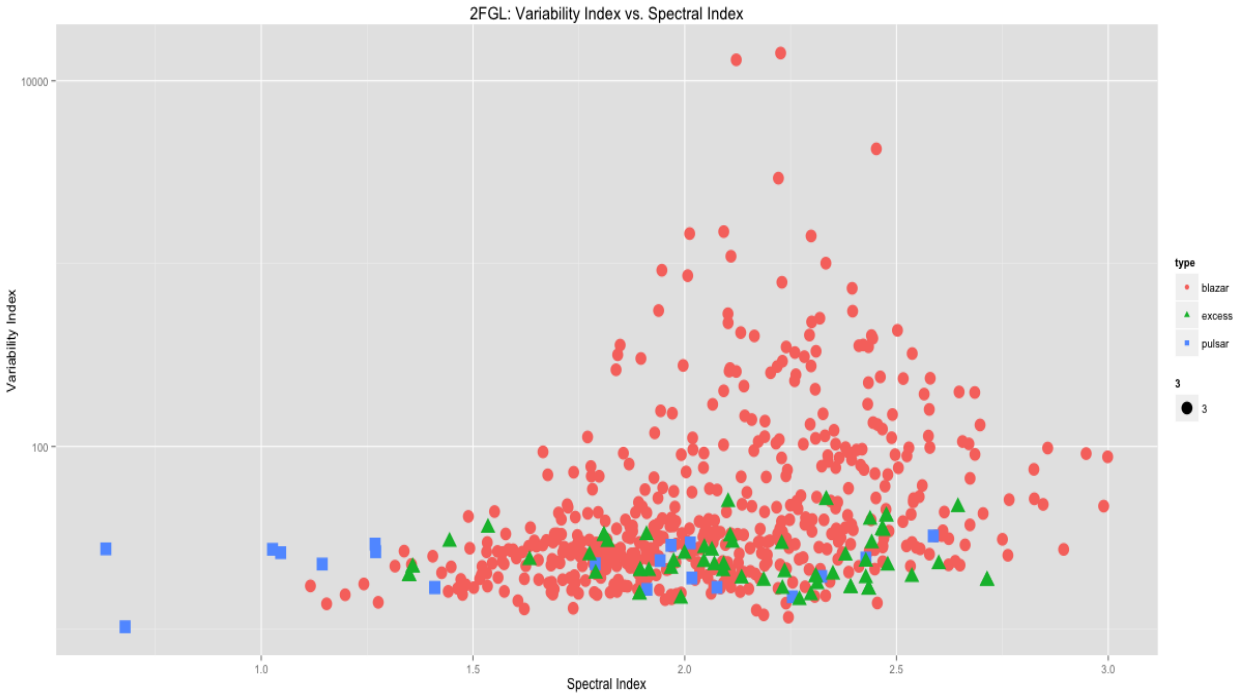


Figure 29: 2FGL – Variability Index vs. Spectral Index

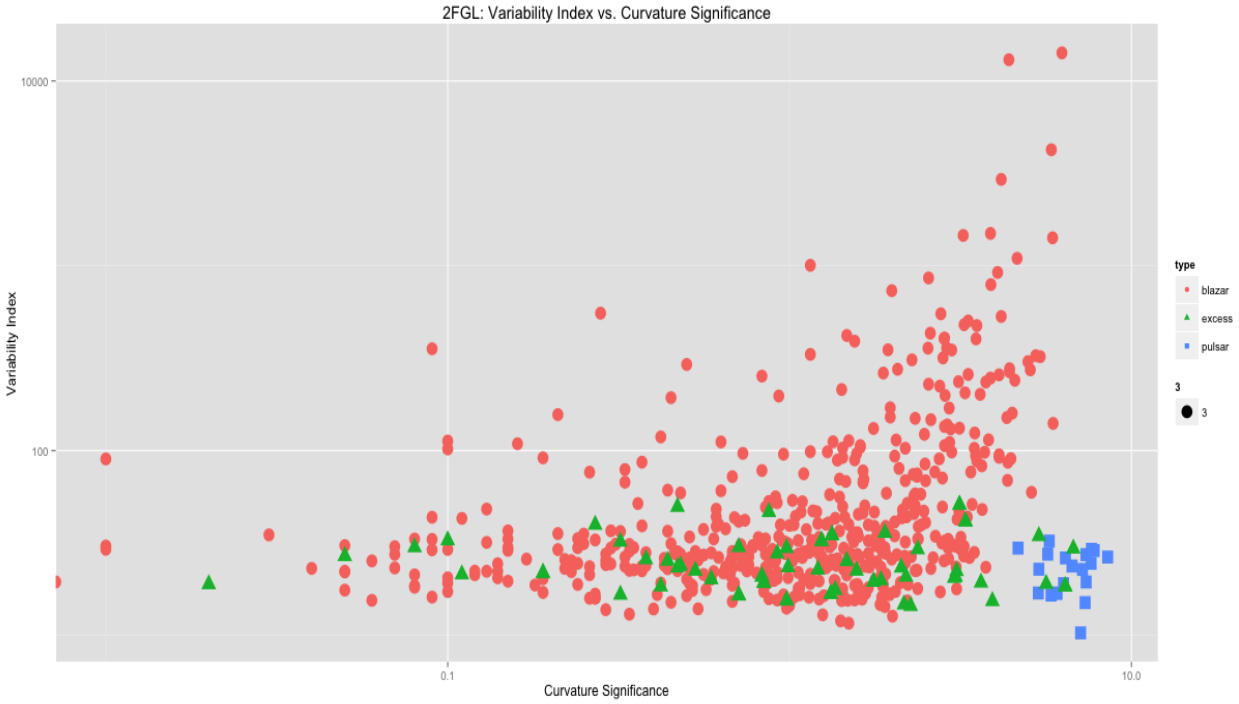


**Figure 30: 2FGL – Variability Index vs. Curvature Significance**

# Appendix B

## 1FGL Individual Plots After Association

This appendix is similar to Appendix A in that it displays the individual plots shown in the pairs plot of Figure 10. These plots are useful in that we can check that our kknn analysis was reliable in properly separating the data. In these plots the red circles signify known blazars, the blue squares signify known pulsars, the green triangles signify unassociated objects identified through kknn analysis as blazars, and the purple crosses signify unassociated objects identified through kknn analysis as pulsars.

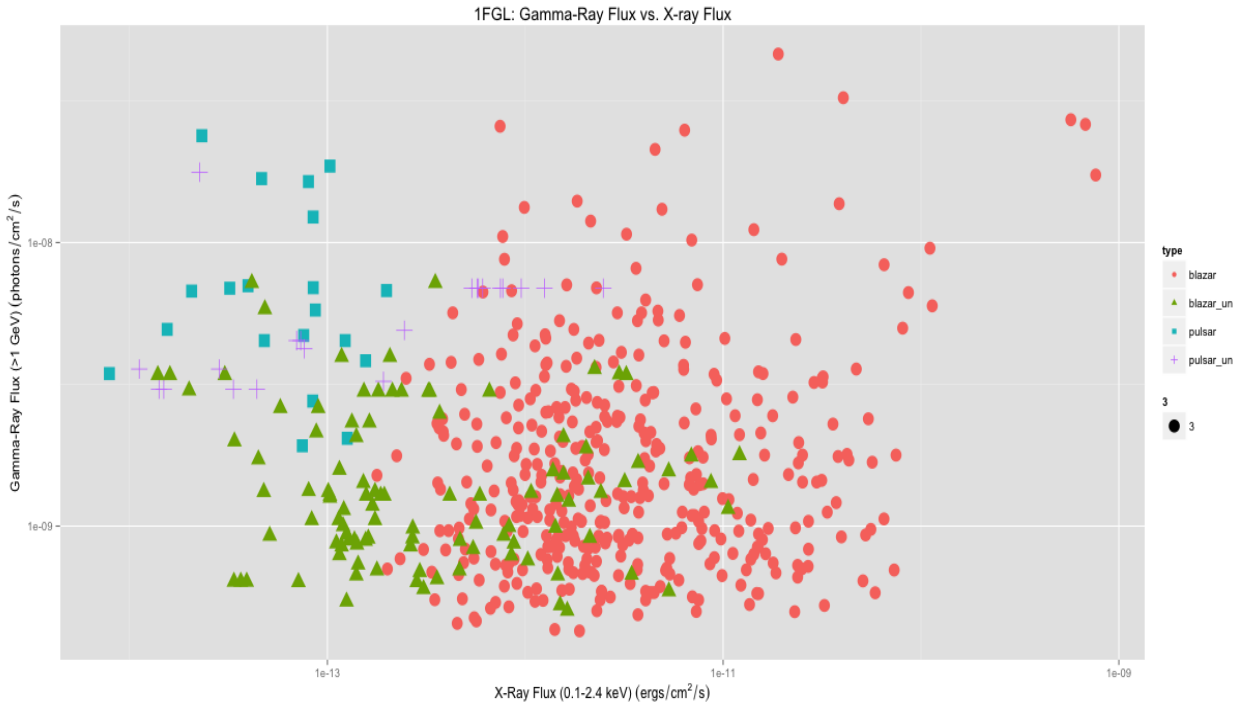


**Figure 31: 1FGL associations – Gamma-Ray Flux vs. X-ray Flux**

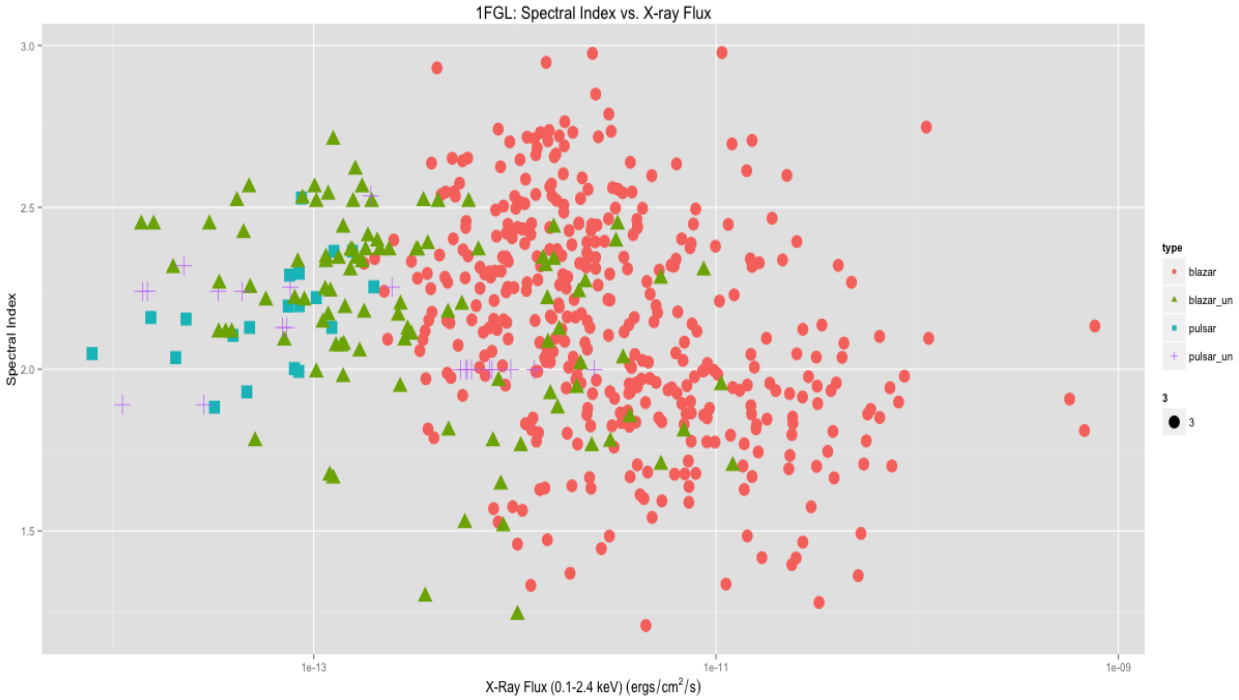


**Figure 32: 1FGL associations – Spectral Index vs. X-ray Flux**

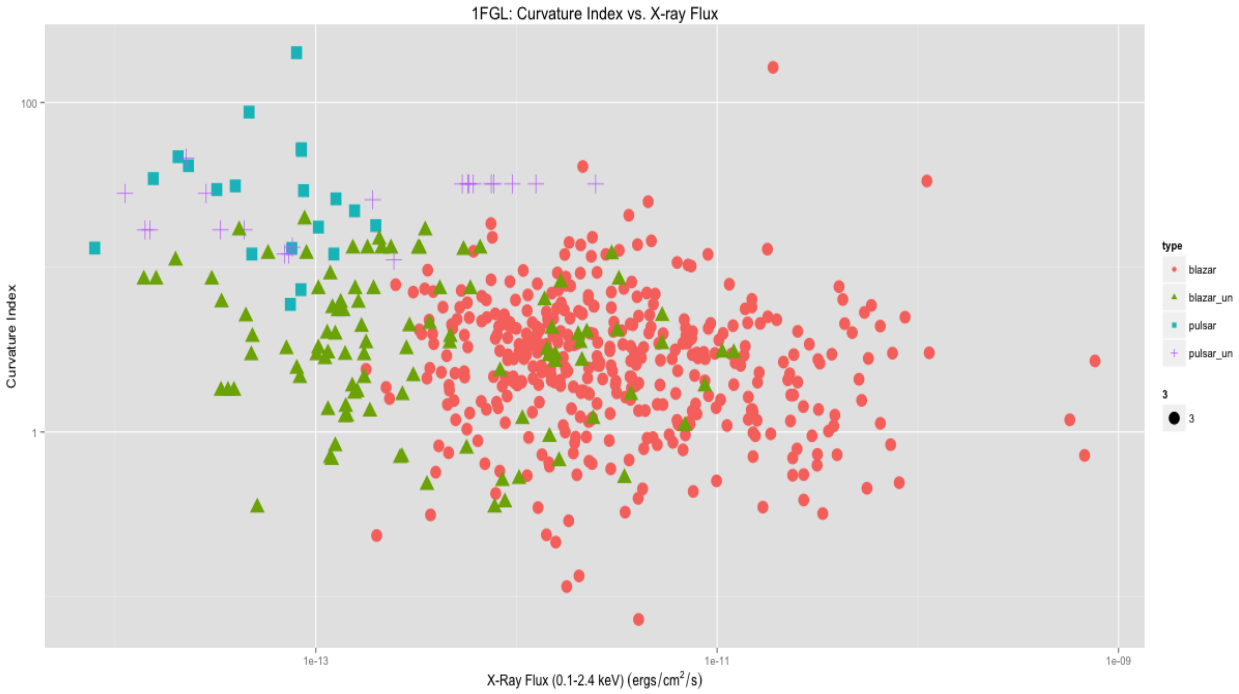


**Figure 33: 1FGL associations – Curvature Index vs. X-ray Flux**

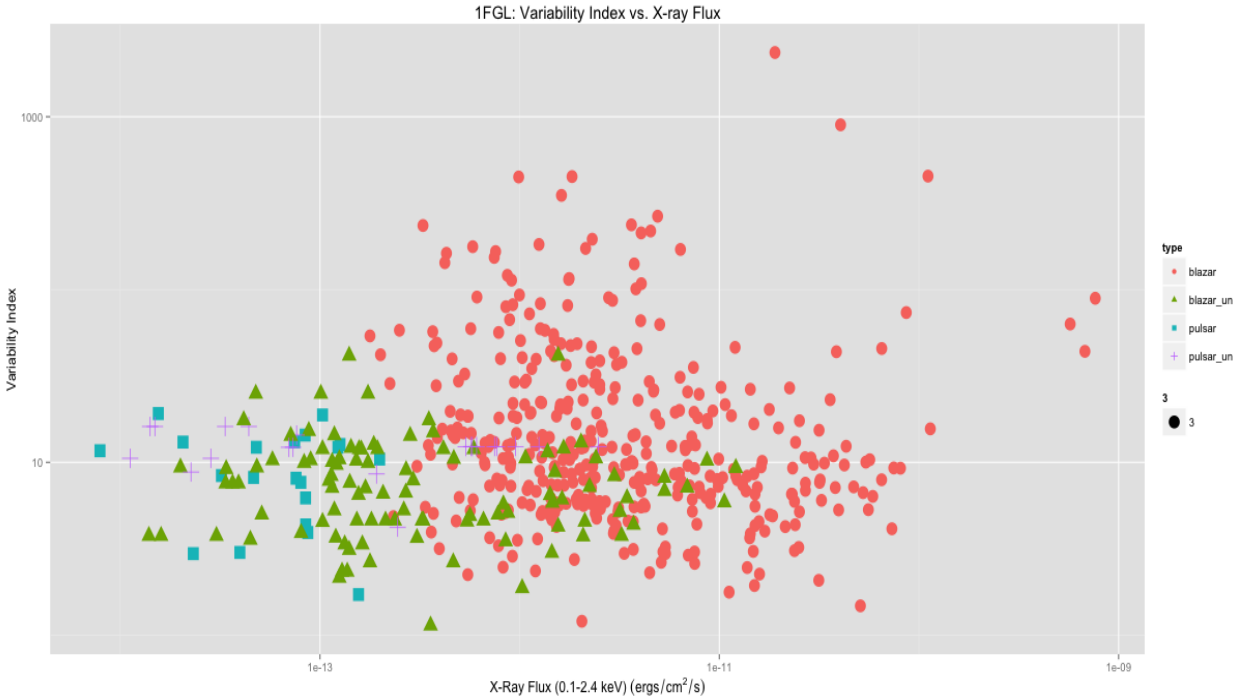


**Figure 34: 1FGL associations – Variability Index vs. X-ray Flux**

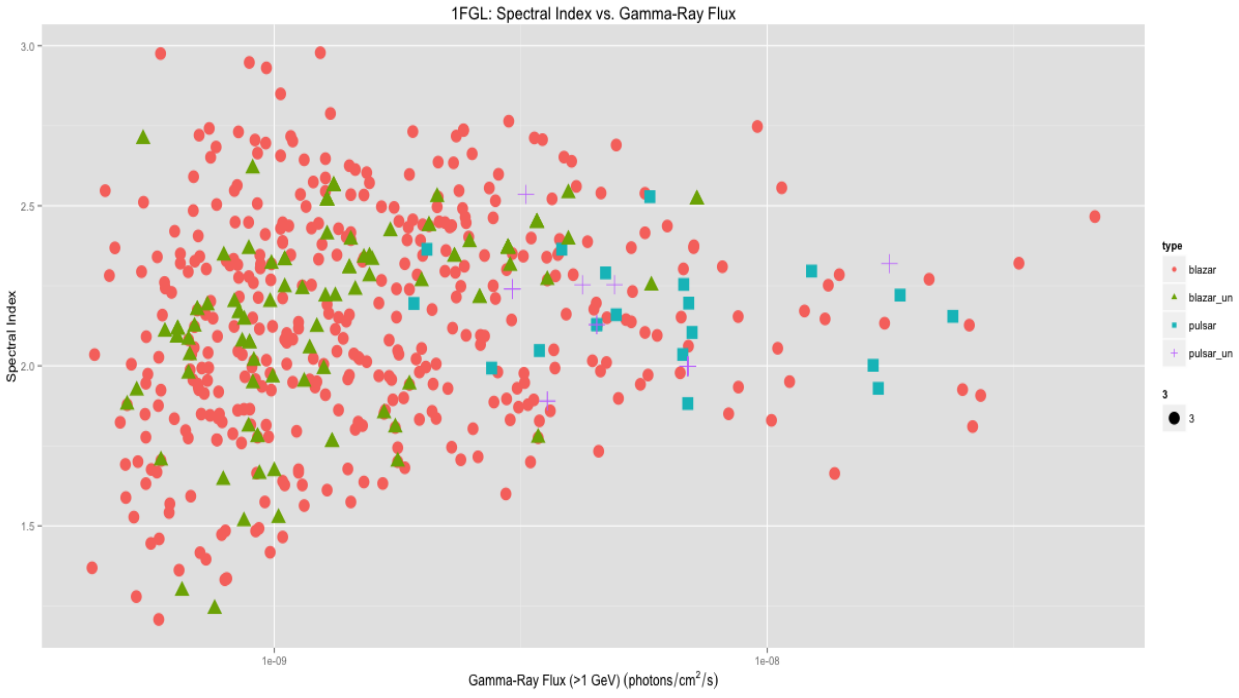


**Figure 35: 1FGL associations – Spectral Index vs. Gamma-Ray Flux**

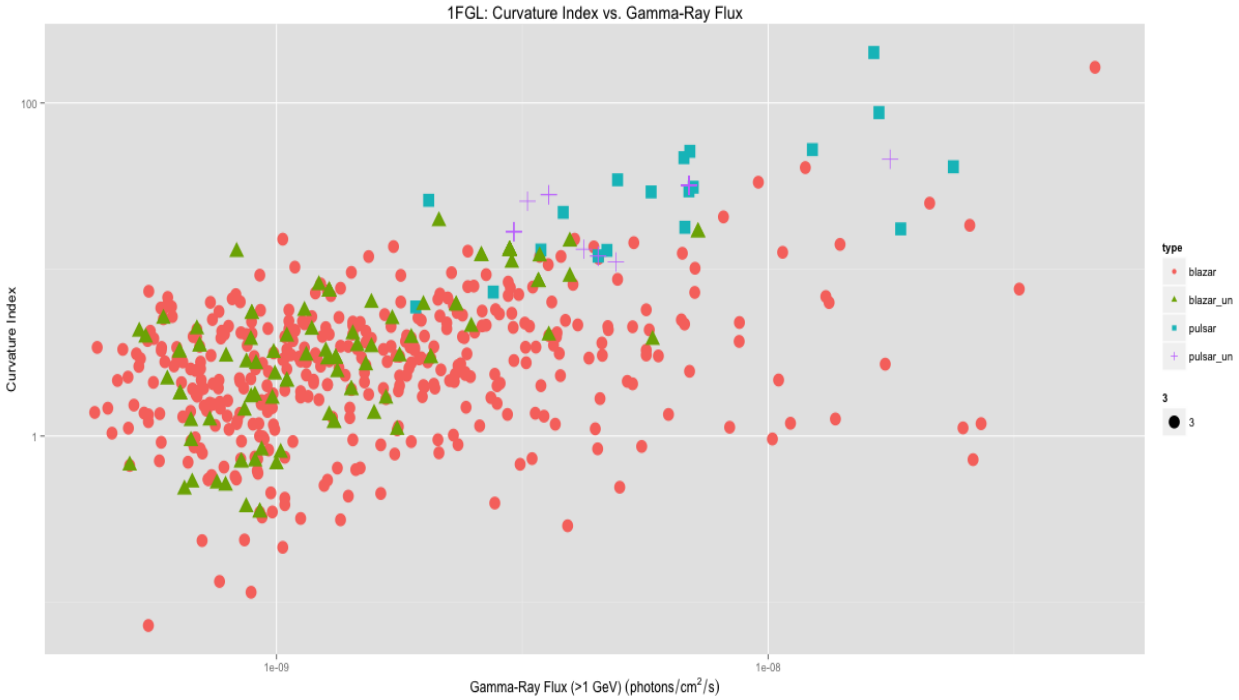


**Figure 36: 1FGL associations – Curvature Index vs. Gamma-Ray Flux**

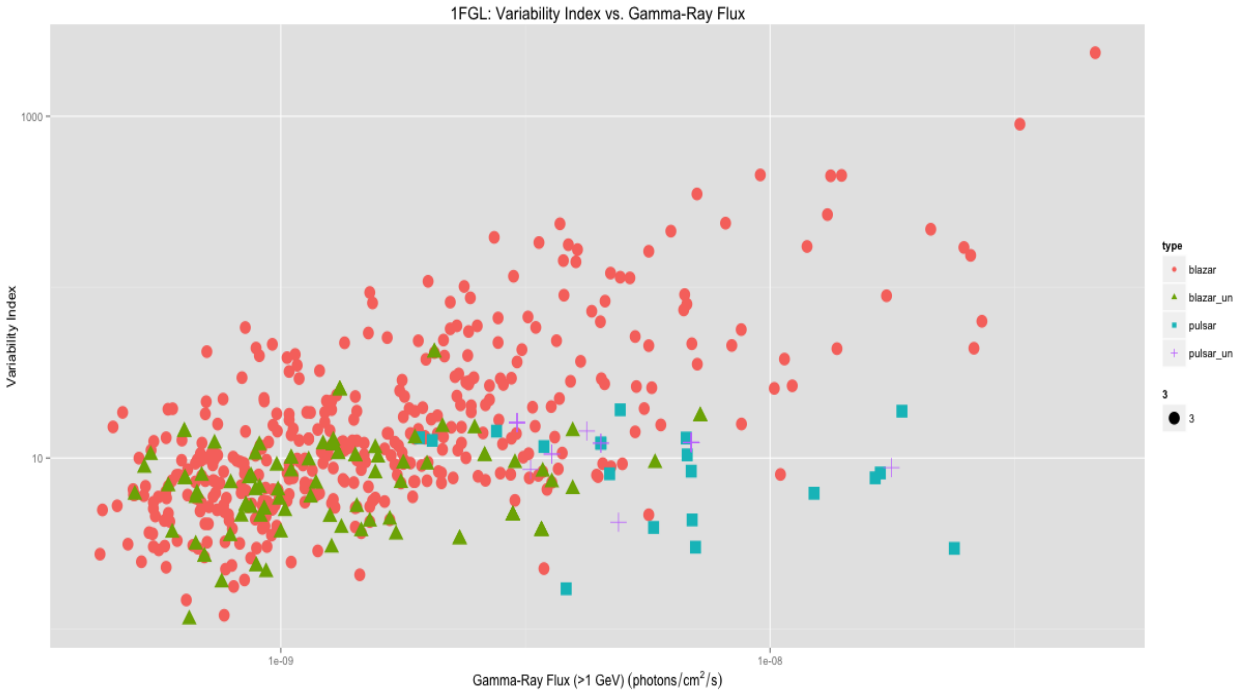


**Figure 37: 1FGL associations – Variability Index vs. Gamma-Ray Flux**

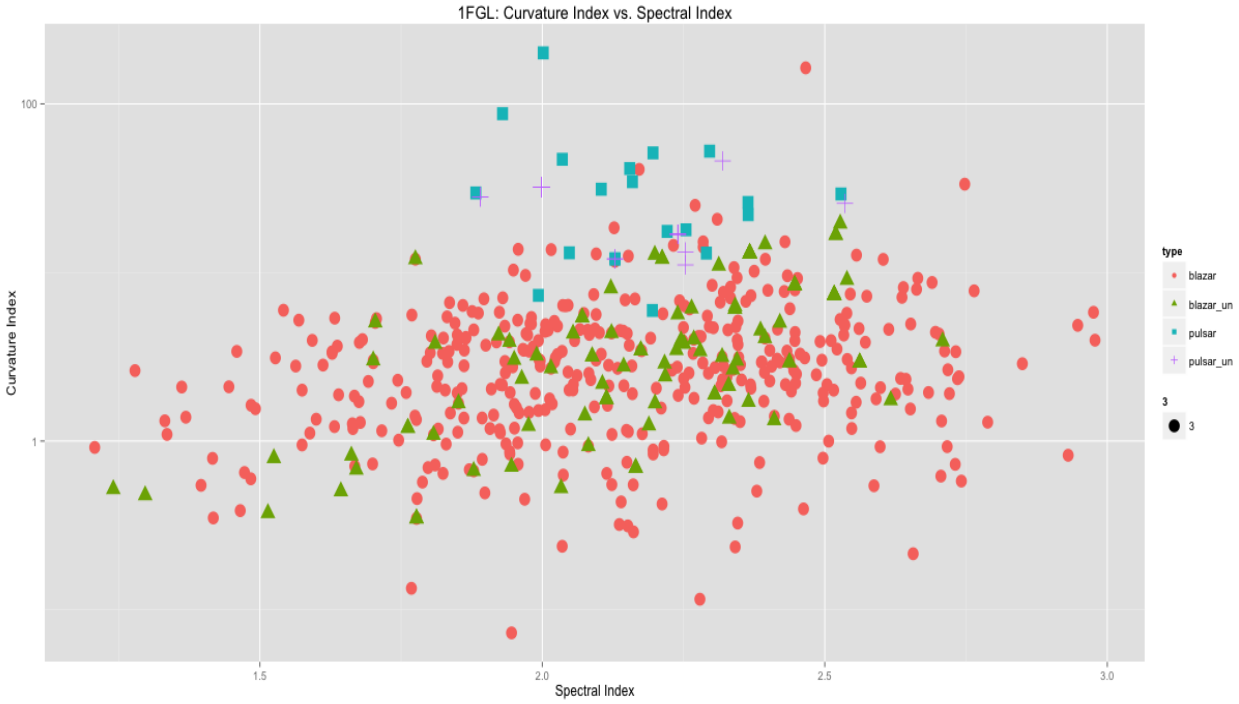


**Figure 38: 1FGL associations – Curvature Index vs. Spectral Index**


**Figure 39: 1FGL associations – Variability Index vs. Spectral Index**

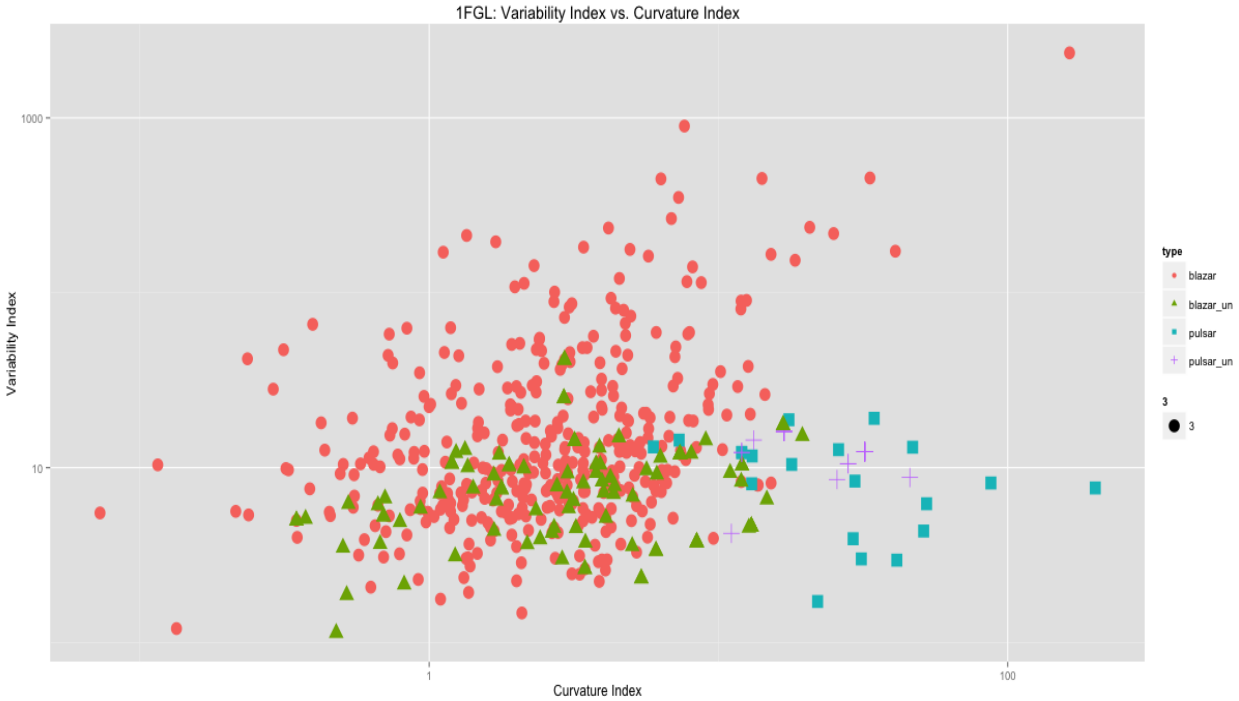


**Figure 40: 1FGL associations – Variability Index vs. Curvature Index**

## BIBLIOGRAPHY

Abdo, A. A., Ackermann, M., Agudo, I. et al., 2010a, ApJ, 716, 30

Abdo, A. A., Ackermann, M., Ajello, M., et al. 2010b, ApJS, 188, 405A

Acero, F., Ackermann, M., Ajello, M., et al., 2015, arXiv: 1501.02003v1

Ackermann, M., Ajello, M., Allafort, A. et al. 2012 ApJ, 753, 83

Ackermann, M., Ajello, M., Atwood, W. B., 2015, arXiv: 1501.06054

Atwood, W. B., Abdo, A. A., Ackermann, M., et al. 2009, ApJ, 697, 1071

Bignami, G. F., Boella, G., Burger, J. J., et al. 1975, Space Science Instrumentation, 1, 245

Burrows, D.N., Hill, J.E., Nousek, J.A., et al., 2005, Sp. Sci Rev, 120, 165

Camilo, F., Kerr, M., Ray, P. S., et al., 2012, ApJ, 746, 39C

Catanese, M., Bradbury, S., M., Breslin, A., C., et al. 1997, ApJ , 487, L143

Cognard, I., Guillemot, L., Johnson, T. J., et al., 2011, ApJ, 732, 47C

Doert, M. & Errando, M. 2014 ApJ, 782, 41

Donnarumma, I., Vittorini, V., Vercellone, S., et al. 2009, ApJ, 691, 13

Hassan, T., Mirabal, N., Contreras, J. L., Oya, I. 2013 MNRAS, 428, 220

Kalberla, P. M. W., Burton, W. B., Hartmann, D., et al. 2005, A&A, 440, 775

Kataoka, J., Yatsu, Y., Kawai, N., et al., 2012, ApJ, 757, 176K

Kerr, M., Camilo, F., Johnson, T. J., et al., 2012, ApJ, 748L, 2K

Kraushaar, W. L., Clark, G. W., Garmire, G. P., et al. 1972, ApJ, 177, 341

Meegan, C., Lichti, G., Bhat, P. N., et al. 2009, ApJ, 702, 791

Mirabal, N.; Fr´ıas-Martinez, V.; Hassan, T.; Fr´ıas-Martinez, E. 2012, MNRAS, 424L, 64

Nolan, P. L., Abdo, A. A., Ackermann, M., et al. 2012, ApJS, 199, 31N

Pian, E., Vacanti, G., Tagliaferri, G., et al., 1998, ApJ, 492, L17

Pletsch, H. J., Guillemot, L., Allen, B., et al., 2012, ApJ, 744, 105P

R Core Team, 2014. R: A language and environment for statistical computing. R Foundation for Statistical Computing, Vienna, Austria. URL http://www.R-project.org/

Ransom, S. M., Ray, P. S., Camilo, F., et al., 2011, ApJ, 727L, 16R

Romani, R. W., Filippenko, A. V., & Cenko, S. B., 2014, ApJ, 793L, 20R

Sambruna, R. M., Aharonian, F. A., Krawczynski, H., et al. 2000, ApJ, 538, 127

Schliep, K. & Hechenbichler , K., 2014. kknn: Weighted k-Nearest Neighbors. R package version 1.2-5. http://CRAN.R-project.org/package=kknn

Schloerke, B., Crowley, J., Cook, D., et al., 2014. GGally: Extension to ggplot2.. R package version 0.5.0. http://CRAN.R-project.org/package=GGally

Stroh, M.C. & Falcone, A.D., 2013, ApJS, 207, 28

Takahashi, Y., Kataoka, J., Nakamori, T., et al., 2012, ApJ, 747, 64T

Thompson, D. J., Bertsch, D. L., Fichtel, C. E., et al. 1993, ApJS, 86, 629

Venables, W. N. & Ripley, B. D., 2002, Modern Applied Statistics with S. Fourth Edition. Springer, New York. ISBN 0-387-95457-0

Wickham, H., 2009, ggplot2: elegant graphics for data analysis. Springer New York.

Zhang, L. & Cheng, K. S., 2003, A&A, 398, 2

# MATTHEW PRYAL – ACADEMIC VITA

401 Oakwood Ave., State College, PA 16803 | Email: mvp5278@psu.edu | Phone: (570)-309-7329

## EDUCATION

Aug 2011-Present **The Pennsylvania State University** - University Park, PA
Schreyer's Honors College – Eberly College of Science
*Bachelor of Science*: Astronomy & Astrophysics
Minors: Physics, Mathematics
Expected Graduation Date: May 2015

## RESEARCH EXPERIENCE

Oct 2012-Present **Research Assistant** – PSU Astronomy & Astrophysics Dept.
Research Advisor: Dr. Abraham Falcone

- Research fast variability of active galactic nuclei using data from the Swift X-ray telescope.
- Research and catalog data on Fermi unassociated sources using Swift data
- Analyze data using IDL programming language
- Publically present data through scientific publications and poster presentations
- Identify unassociated Fermi sources using X-ray data from Swift

## PUBLICATIONS AND PRESENTATIONS

Pryal, M., Falcone, A., Stroh, M., *"A Search for Fast X-ray Variability from Active Galactic Nuclei Using Swift,"* 2015, ApJ, 802, 33; arXiv:1501.07288

Pryal, M., Falcone, A., Stroh, M., *"Using Swift to Search for Fast X-ray Variability from Blazars and Study Jet Emission"*, 2014, AAS, 223, 250.05

Falcone, A., Pryal, M., Stroh, M., *"Probing Fast X-ray Variability of Blazars with a Large Data Set from Swift"*, 2014, HEAD, 14, 106.15

Falcone, A., Stroh, M., Pryal, M., *"Using Swift to Obtain X-ray Monitoring of Fermi Blazars and X-ray Counterparts to Fermi Unassociated Sources"*, 2014, AAS, 223, 301.05

## HONORS

- Penn State Dean's List – seven consecutive semesters (Aug 2011-present)
- Penn State Schreyer's Honors College member
- Penn State Schreyer's Honors College Gateway Scholar
- Awarded $1,000 Science Travel Grant – Penn State Eberly College of Science
- Awarded Kadtke Family Endowed Scholarship (2013, 2014) – Penn State Eberly College of Science

## EXTRACURRICULARS

- **Volunteer Work**
  - Astrofest with PSU Astronomy Department (2012, 2013, 2014)
    - Led kids activities, performed 3D Mars shows, helped with rooftop observing, helped with all other demonstrations
  - Exploration U with PSU Astronomy Department (2012, 2013, 2014)
    - Ran multiple astronomy demonstrations for the public including scale of the solar system, crater demonstrations, and comet making
  - Run Stargazing Open House at PSU with Astronomy Club (2012-present)
    - Set up and monitor telescopes, educate public on objects observed
  - Haunted U run by Penn State's Science U (2013, 2014)
    - Led group of about 10 students in grades K-2 through science demonstrations that highlight "magical" science
  - Think Outside the Beaker run by Penn State's Science U (2013, 2014)
    - Prepared and led demonstrations for middle school students highlighting the fundamental forces of nature as well as astronomy observing techniques
  - Mars 3D shows for the public (June 2014-present)
    - Present shows for the public outlining a 3D tour of the planet Mars. Shows are presented for groups such as scout troops, classes on field trips, Penn State students, and others that request shows.
  - Altar Server at home church (2004-2011)
    - Helped throughout the community in events such as: church picnics, Feed-A-Friend, food drives, clothes drives, etc.
- **Vice President – Penn State Astronomy Club** (Aug 2013-present)
  - Create fun and interactive bi-weekly meetings for club members
  - Perform public outreach in and around the Penn State community
- **Penn State Intramural Sports**
  - Racquetball, Golf, Softball, Volleyball, Mushball, Kickball, Bocce Ball
  - IM Racquetball Champion – Spring 2015